CHAPTER 6

In vitro Acid Phosphatase Inhibition by Oxido- and Mixed-Ligand Peroxido-Niobium(V) Complexes

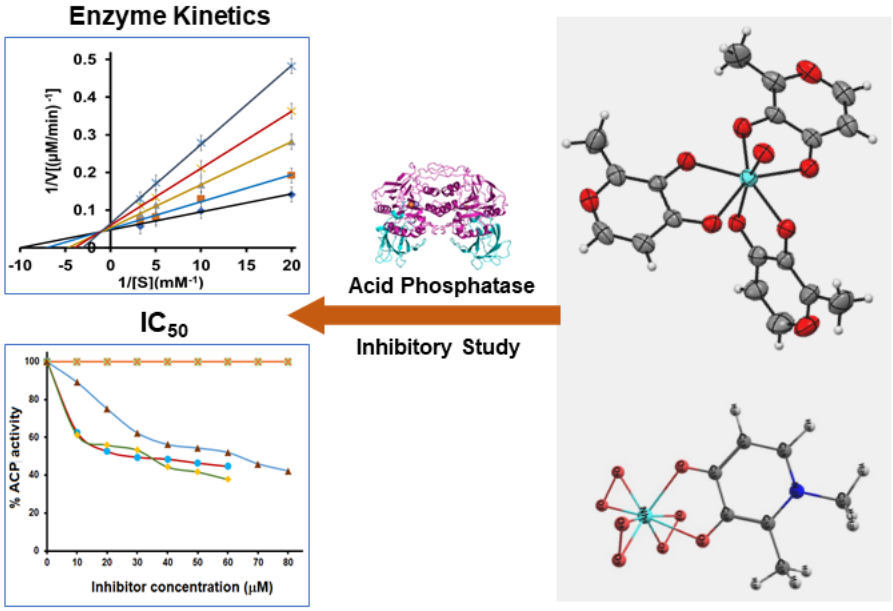

6.1 Introduction

Niobium being a bioinert and non-toxic metal with a very high LD_{50} value [1,2], utility of Nb-based materials in the field of medicinal and biological chemistry is not new. Oxides of niobium have been documented to be chemically and thermally stable, biocompatible, and hypoallergenic materials with great biological features [1]. Markedly, vanadate and niobate have been reported as strong inhibitors of the sarcoplasmic reticulum (SR) Ca^{2+}-ATPase that can influence a variety of cellular processes, including calcium homeostasis [3]. Design and synthesis of water-soluble Nb(V)-based compounds still remains a notable challenge and a matter of great demand mainly due to their potential use as precursors for obtaining Nb-based oxide materials for advanced technology implementations [4,5]. In fact, peroxidoniobates have been recognized as water-soluble valued precursors for developing Nb-based oxide materials [4,5]. However, in spite of Nb being a member of the same periodic group as vanadium, the paucity of reports pertaining to the biological activity of peroxidoniobium (pNb) compounds [6-8] appears to be indeed intriguing. Synthetic compounds of vanadium, including peroxidovanadates, notwithstanding their low hydrolytic stability under the physiological condition and toxicity [9-11], continue to garner enormous importance as insulin-enhancing, anti-neoplastic agents with well-documented enzyme inhibitory activity [9-14].

As evident from a survey of relevant literature, the identification of phosphatase inhibition as one of the significant pathways [15,16] associated with the insulin like activity of vanadium derivatives [16,17], stimulated an extensive exploration of a diverse range of vanadium compounds as phosphatase inhibitors [11,13,14]. Apart from the expected therapeutic potential of the phosphatase inhibitors [13,16,18], as a class of enzymes phosphatases play vital roles in many signal transduction mechanisms [13,16,18,19]. McLauchlan *et al*. [18], in a recent comprehensive review on phosphatase inhibition by vanadium species, have observed that in majority of the reports, the inhibitory efficiency of the tested vanadium compounds has been determined in terms of EC_{50} (relative inhibitory potency) values whereas, very few studies described mechanism of such inhibition with defined inhibitory constant (K_i) values [18].

Relevant here is to mention that during the past decade, our research group has developed a series of mononuclear, dinuclear and macromolecular peroxido compounds of metals of groups V and VI and investigated several of their biochemically relevant features [20-30] including their activity with enzymes such as catalase [24-28], alkaline

phosphatase (ALP) [25,26,29], acid phosphatase (ACP) [27-29], and calcineurin [30]. Importantly, most of these structurally defined compounds were observed to be stable under physiological condition and displayed extraordinary resistance to degradation under the action of catalase [24-28]. Interestingly, a recent comparative study carried out in our laboratory revealed that peroxidotantalum complexes were significantly more potent inhibitors of acid phosphatase *vis-à-vis* their peroxidovanadate analogs [28]. In another recent study, other members from our group have shown for the first time that V and Nb peroxido complexes anchored to poly(acrylate) can serve as equally potent uncompetitive inhibitors of the activity of calcineurin, a serin threonine protein phosphatase [30].

In view of the above background and consistent with the ongoing efforts of our research group focused on developing biologically relevant metal complexes, we sought to develop a set of new mixed-ligand complexes of Nb(V) using a combination of O,O-donor ligands, *viz*., peroxido, maltol and deferiprone. We considered the biogenic, non-toxic metal chelators such as maltol (3-hydroxy-2-methyl-4-pyrone) and deferiprone (3-hydroxy-1,2-dimethylpyridin-4-one) as the appropriate choice of ligands for the present study. With an inherent ability to form both σ and π bonds with metal ions, these hydroxypyrone and hydroxypyridone ligands with nearly similar chelating abilities have been known to form stable metal complexes with significant bio-relevant characteristics like charge neutrality, hydrolytic stability, lipophilicity and water solubility [31-34]. In addition to being widely known as a clinically important Fe chelator, deferiprone acts as an effective ligand to a range of metals, including Ga, Al, Zn, Cu, and especially Fe [35,36]. Maltol and deferiprone complexes of V(III) such as $V(malt)_3$ and $V(def)_3 \bullet 12H_2O$ were reported to display significant anti-proliferation activity towards different cancer cells as well as insulin enhancing ability [33,37]. There are scores of reports documenting bio-medical application of metal-maltol complexes, *viz*., ferric maltol complex has been effectively implemented in the treatment of iron-deficiency anaemia [38] and Al(III)-maltol complex was applied in the study of neurological disorder like Alzheimer's disease [39]. Apart from that, mixed ligand organomercury(II) as well as oxidoperoxidomolybdenum(VI) complexes coordinated to maltol have been found to display antibacterial properties against various pathogenic strains [40,41]. Most significantly, neutrally charged water-soluble bis(maltolato)oxidovanadium(IV) complex (BMOV), has been recognized as the benchmark compound for its potent glucose- and lipid-lowering insulin-mimetic properties [42,43]. The complex has also been clinically

tested as an effective oral antidiabetic drug formulation [42,44]. Additionally, V(IV) and V(V) complexes of maltol were observed to regulate *in vitro* alkaline phosphatase activity and osteoblast-like cell growth [45]. Surprisingly, notwithstanding these important findings, no report seems to exist till date dealing with maltol-containing Nb-derivatives.

In this chapter, we describe the synthesis and characterization of two new mixed-ligand triperoxido niobium(V) complexes (**6.2** and **6.3**) with a maltol (malt) or deferiprone (def) as a co-ligand as well as the facile synthesis and structural characterization of a heretofore unreported neutral complex tris(maltolato)oxidoniobium(V) complex (**6.1**). Moreover, we present here the results of our comparative kinetic investigation on *in vitro* phosphatase inhibitory activity of a structurally diverse set of Nb(V) complexes comprising of newly synthesized neutral oxidoniobium complex **6.1**, the peroxido complexes **6.2** and **6.3** along with the peroxidoniobium-containing macromolecular complexes, $[Nb(O_2)_3(carboxylate)]^{2-}$-PMA (**4.1**) (Chapter 4).

6.2 Experimental section

6.2.1 Synthesis of the complex, $[NbO(malt)_3]_2 \cdot 9H_2O$ (6.1)

Addition of a methanolic solution of maltol (2 mmol in 5 mL methanol) to a solution of Niobium(V) chloride (0.27 g, 1 mmol) in 5 mL of methanol at room temperature yielded a greenish-yellow coloured solution. After stirring the solution for 24 h at room temperature, 4 mL of water was added to it, and the solution was warmed slightly to obtain a clear solution. The solution was then allowed to cool to room temperature, and a few drops of acetone (*ca*. 1 mL) were added to it. On keeping this solution for slow evaporation at room temperature, colourless crystals suitable for single crystal XRD analysis were obtained within 4-5 days.

Solubility of the complex in water: 560 mg/L, methanol: 5600 mg/L, acetonitrile: 4800 mg/L and ethanol: 1600 mg/L.

6.2.2 Synthesis of the complex $Na_2[Nb(O_2)_3(malt)] \cdot H_2O$ (6.2)

First, the precursor complex $Na_3[Nb(O_2)_4] \cdot 13H_2O$ (**TpNb**) was prepared by adopting a reported method (Chapter 3, section 3.2.2) [46]. For the synthesis of **6.2**, maltol (0.16 g, 1.25 mmol) was added to a constantly stirred solution of the precursor complex **TpNb**, (0.65 g, 1.25 mmol) prepared by dissolving it in 4 ml of 30% H_2O_2, under ice-bath condition. The resulting clear solution of pH *ca*. 7 was allowed to stand for 3 h at <4 ºC.

When acetone was added to this solution, a white pasty mass precipitated out from it. The product was obtained as microcrystalline solid after repeated treatment with acetone under scratching and centrifuging at high rpm. It was then dried and stored in a vacuum desiccator.

6.2.3 Synthesis of the complex $Na_2[Nb(O_2)_3(def)]\cdot 2H_2O$ (6.3)

Addition of deferiprone (0.17 g, 1.25 mmol) to a solution of **TpNb** (0.65 g, 1.25 mmol) in 30% hydrogen peroxide (4 ml, 35 mmol) at a temperature <4 ºC yielded a colourless solution of pH *ca*. 12. Few drops of dilute nitric acid (2 N, 1.2 mL) was added to the reaction until the pH was adjusted to 7. The greenish-yellow solution obtained was kept undisturbed for 3 h in an ice bath. A white pasty precipitate was obtained when acetone was added to the solution. The white microcrystalline compound was extracted by further scratching, washing with acetone, and centrifuging at high rpm. It was then vacuum dried, and stored.

6.2.4 X-Ray Crystallography

X-ray intensity data from a Bruker SMART APEX II single crystal X-ray CCD diffractometer with graphite-monochromatized Mo-Kα (= 0.71073 Å) radiation at 100 K determined the molecular structure of the complex $[NbO(malt)_3]_2\cdot 9H_2O$. SHELXS-97 and SHELXL-2014/7 directly resolved the data [47]. The graphics interface package was PLATON, and the figures were generated using ORTEP 3.07 and Mercury 3.8 [48]. Direct method was used to solve the structure. Difference maps and anisotropic refinement were used to locate the remaining atoms. Geometrically fixed hydrogen atoms bound to carbon were refined with isotropic thermal parameters, usually 1.2 U_{eq} of their parent atoms. **Table 6.1** shows crystallographic data for the complex.

Table 6.1: Crystal data and structure refinement details for $[NbO(malt)_3]_2\cdot 9H_2O$ (**6.1)**

	6.1
Sum formula	$C_{36}H_{30}Nb_2O_{29}$
Formula weight	1112.42
Temperature (K)	100(2)
Wavelength (Å)	0.71073
Crystal system	Orthorhombic

Continued…

	6.1
Space group	*Pbcn*
a(Å)	22.3770(14)
b(Å)	13.3328(8)
c(Å)	15.5757(8)
Volume ($Å^3$)	4647.0(5)
Z	4
D_c ($g.cm^{-3}$)	1.590
Reflections collected	46157
Goodness-of-fit on F^2	0.974
Final R indices [I>2σ (I)]	0.0495, wR_2 = 0.1237
R indices (all data)	0.0966, wR_2 = 0.1481
CCDC deposition no.	2149737

6.2.5 Computational Details

Structures of the pNb complexes $Na_2[Nb(O_2)_3(malt)]\cdot H_2O$ (**6.2**) and $Na_2[Nb(O_2)_3(def)]\cdot 2H_2O$ (**6.3**) were modelled using the molecular building and visualization tool Gauss View and the Density Functional Theory (DFT) calculations were executed using the Gaussian 09 program package [49]. Energy minimization of the complexes was done employing a more popular local density functional M06-2X without imposing any symmetry constraints [50]. The Minnesota functional M06-2X developed by Zhao and Truhlar gives good results for both the main group as well as transition metals by establishing the dependency of the exchange-correlation energy on local spin density, spin density gradient, and spin kinetic energy density [51]. A density-fitting triple-ζ valence with double polarization def2-TZVPP basis set is employed for all atoms to locate their atomic orbitals [52]. Absence of imaginary frequencies (NIMAG=0) confirmed the structures to be true minima's on the PES.

6.2.6 Stability of the pNb complexes in aqueous solution

The stability of the pNb complexes in solution was determined by preparing an aqueous 100 mL, 0.2 mM stock solution of the respective complexes with weighed amounts such as **6.2** (0.076 mg/mL), **6.3** (0.082 mg/mL) and **4.1** (0.150

mg/mL) maintaining various pH values- pH 8.0, 7.0 and 4.6 in phosphate buffer (50 mM). The peroxide amount in aliquots withdrawn at a regular time gap from that solution was estimated by iodometric titration throughout 12 h. Furthermore, ^{1}H and ^{13}C NMR analyses of the complexes were conducted over 12 h for any probable changes (**Fig. 6.16** and **6.17**).

6.2.7 Acid phosphatase activity measurement

The ACP activity was assessed spectrophotometrically using the substrate *p*-nitrophenyl phosphate (*p*-NPP) [29,53-55] in a standard assay mixture of 0.1 M acetate buffer (pH = 4.6), ACP (18.38 μg protein mL^{-1}), and Nb(V) inhibitors with different concentrations of the inhibitors in the range of: 1-10 μM for **4.1** and 10-80 μM for **6.1-6.3** as shown in **Fig. 6.19**. In the case of the macro-complex, the concentrations used was based on metal loading (mmol Nb g^{-1} of the polymer). The reaction was initiated by adding *p*-NPP to the pre-incubated (at 30 °C for 5 min) test solution and terminated after incubating for 30 min at 30 °C by the addition of 0.5 M, 0.9 mL solution of NaOH. In the test solution, the amount of *p*-NPP converted to *p*-nitrophenol (*p*-NP) by ACP was ascertained by recording its absorbance at 405 nm ($\varepsilon_{p\text{-nitrophenolate}}$ = 18000 M^{-1} cm^{-1}) [56]. Enzyme activity under inhibitor-free condition was determined in a control experiment. The IC_{50} for each inhibitor causing 50% inhibition of ACP activity was graphically determined. The results depicted in the figures are in the average ± SE from the triplicate experiments.

6.2.8 Determination of kinetic parameters

The enzyme kinetic assays were performed using the substrate (*p*-NPP) concentration in the 50-300 μM range with different concentrations of inhibitors or without the inhibitor species (**Fig. 6.20**). The maximum velocity (V_{max}), Michaelis constant (K_m), and kinetic constants were calculated from Lineweaver-Burk (L-B) plots derived from the Michaelis-Menten equation [54,57-59].

$$\frac{1}{V} = \frac{K_m}{V_{max}[S]} + \frac{1}{V_{max}} \qquad (\mathbf{6.1})$$

In this work, the following expression was used for the determination of the mode of inhibition:

$$V = \left\{ \frac{V_{max} \times [S]}{K_m\left(1 + \frac{[I]}{K_i}\right) + [S]\left(1 + \frac{[I]}{K_{ii}}\right)} \right\} \qquad (\mathbf{6.2})$$

Here *V* refers to velocity, [S] and [I] refer to the concentrations of *p*-NPP and inhibitor, respectively. K_i and K_{ii} are the inhibitory constants for the competitive and non-competitive part, respectively, defined by the linear regression analysis of the secondary plots of the initial rate data. The constant K_i was calculated from the *x*-intercept of the re-plot of the slopes from the L-B plots versus [I], whereas the value of K_{ii} was the *x*-intercept of the plot of intercepts of the L-B plots against [I].

6.3 Results and Discussions

6.3.1 Synthesis

As illustrated in **Scheme 6.1**, the synthesis of new tris(maltolato)oxidoniobium(V) complex was achieved *via* a reasonably straightforward route based on the reaction of $NbCl_5$ with a methanolic solution of maltol, without the use of any deprotonating agent. Slow evaporation of the reaction solution afforded single crystals of $[NbO(malt)_3]_2 \cdot 9H_2O$ (**6.1**) suitable for XRD analysis. On the other hand, the heteroleptic water-soluble pNb complexes with maltol and deferiprone as co-ligands, $Na_2[Nb(O_2)_3(malt)] \cdot H_2O$ (**6.2**) and $Na_2[Nb(O_2)_3(def)] \cdot 2H_2O$ (**6.3**) were obtained by employing a synthetic strategy based on the reaction of pre-synthesized sodium tetraperoxidoniobate (**TpNb**) with the respective co-ligands in the presence of 30% H_2O_2 in an aqueous medium, at near-neutral pH. Unlike the peroxidoniobium complexes **6.2** and **6.3**, which are water soluble, complex **6.1** is partially soluble in water and highly soluble in methanol, acetonitrile and ethanol.

6.3.2 Characterization

The composition of the compounds [presented in **Table 6.2**] derived from ICP-OES and C, H, N elemental analysis was in good agreement with the structural formula assigned to the complexes. From the results of ICP-OES and elemental analysis, the ratio of $Nb:O_2^{2-}$ was found to be 1:3 for the heteroleptic pNb complexes (**6.2** and **6.3**), consistent with the formation of triperoxidoniobium species. The results also confirmed the presence of three maltol ligands per Nb center in complex **6.1.** The occurrence of Nb in the compounds in its +5 oxidation state has been ascertained from the magnetic susceptibility measurements, which revealed that the compounds are diamagnetic.

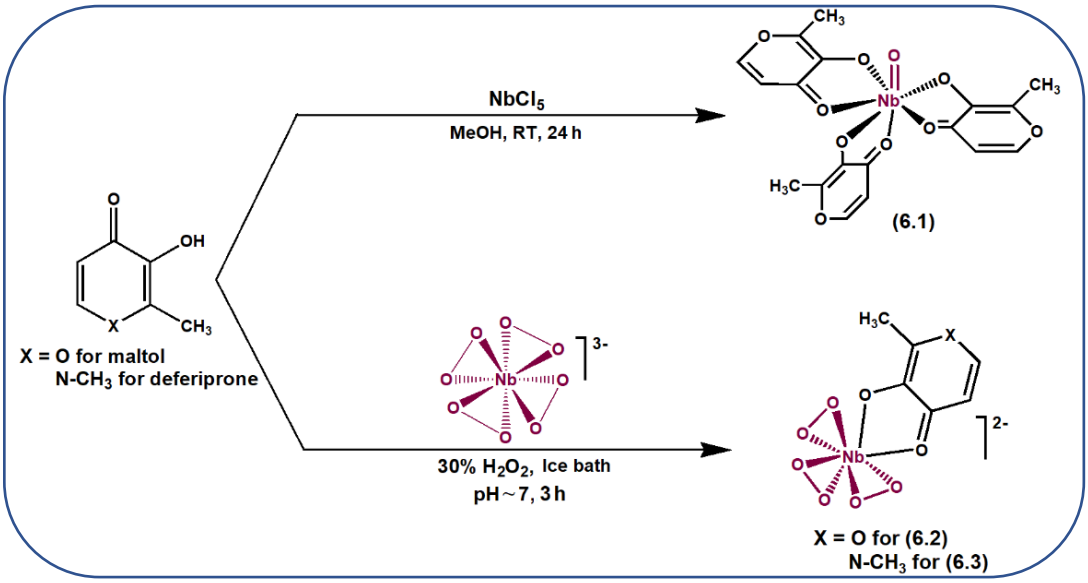

Scheme 6.1 Synthesis of oxidoniobium(V) complex **6.1** and peroxidoniobium(V) complexes, **6.2** and **6.3**.

6.3.2.1 FTIR and Raman spectral analysis

The FTIR spectra of the complexes, along with the respective free ligands, are displayed in **Fig. 6.1** and **6.2**. The complementary Raman spectra of the complexes **6.1-6.3** are presented in **Fig. 6.3**. The IR spectra of the free maltol ligand exhibited typical peaks located approximately at 3260, 2922, and 1655 cm^{-1} attributable to ν(OH), ν(CH_3) and ν(C=O) vibrations, respectively [31,60,61]. In the case of both complexes **6.1** and **6.2**, the stretching vibration corresponding to the -OH group of the ligand disappeared [31,60,61]. This indicated deprotonation of the -OH group and its participation in metal coordination [62]. The complexes showed a new broad peak at *ca*. 3400 cm^{-1}, typical of lattice water [41,61]. Furthermore, shifting of the stretching vibration of the C=O group to a lower wavenumber of 1622 and 1638 cm^{-1} for **6.1** and **6.2**, respectively, suggested the involvement of the carbonyl group in complexation [31,41,60-62]. Similarly, in the case of complex **6.3**, the coordination of niobium to deferiprone through the -OH and C=O groups was confirmed from the absence of the peak at 3147 cm^{-1} and shifting of the stretching vibration of the C=O group from 1630 to 1611 cm^{-1} in the complex [35,63].

Table 6.2: Analytical data for the synthesized Nb(V) complexes

Compounds	% found from elemental analysis/ (Theoretical %)					% O_2^{2-} content (Theoretical %)	Ratio of Nb: O_2^{2-}
	C	H	N	Nb	Na		
6.1	38.28	4.32	-	16.38[a]	-	-	-
	(38.25)	(4.28)	-	(16.44)	-	-	-
6.2	19.12	1.74	-	24.41[a]	12.28[a]	25.67	1:3
	(19.06)	(1.87)	-	(24.58)	(12.16)	(25.40)	
6.3	20.35	2.65	3.19	22.63[a]	11.53[a]	23.68	1:3
	(20.55)	(2.96)	(3.42)	(22.71)	(11.24)	(23.47)	

[a]Determined by ICP-OES analysis

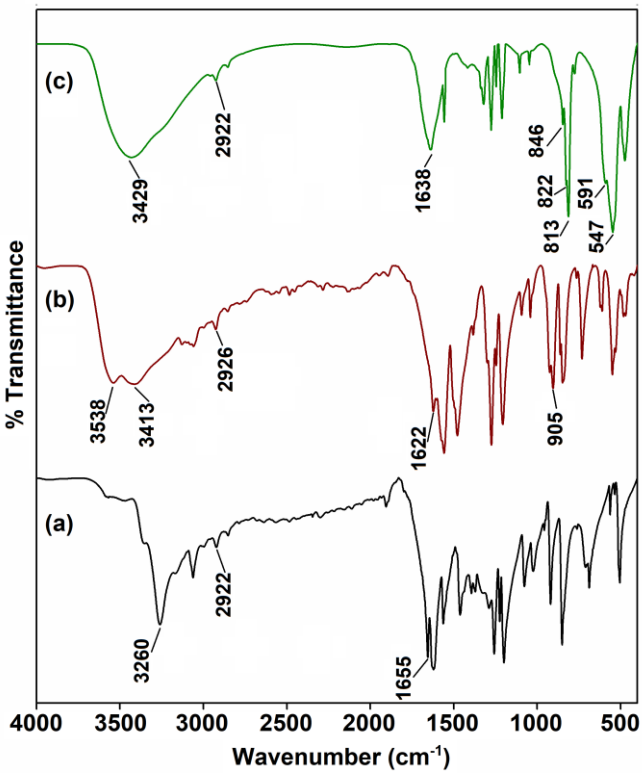

Fig. 6.1 FTIR spectra of (a) **Maltol**, (b) complex **6.1** and (c) complex **6.2**.

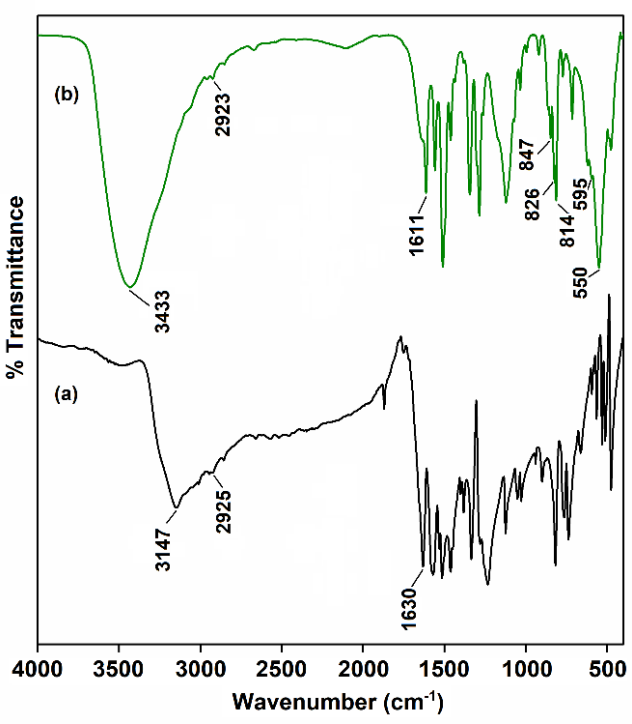

Fig. 6.2 FTIR spectra of (a) **Deferiprone** and (b) complex **6.3**.

In addition to the aforementioned frequencies, the presence of a sharp band at *ca.* 905 cm^{-1} in both IR and Raman spectra of **6.1** testified to the presence of Nb=O moiety in

the complex [63]. In the case of the pNb complexes, a clear indication of the formation of triperoxidoniobium moiety was obtained from the observance of three discrete peaks within the range of 800-900 cm^{-1} in their IR and Raman spectra. The observed pattern is typical of ν(O-O) vibration corresponding to a triperoxidoniobium species [4,64]. In addition, the ν_{asym}(Nb-O_2) and ν_{sym}(Nb-O_2) vibrations corresponding to side-on bound peroxido group [4,64] of the complexes were observed in the 500-600 cm^{-1} region.

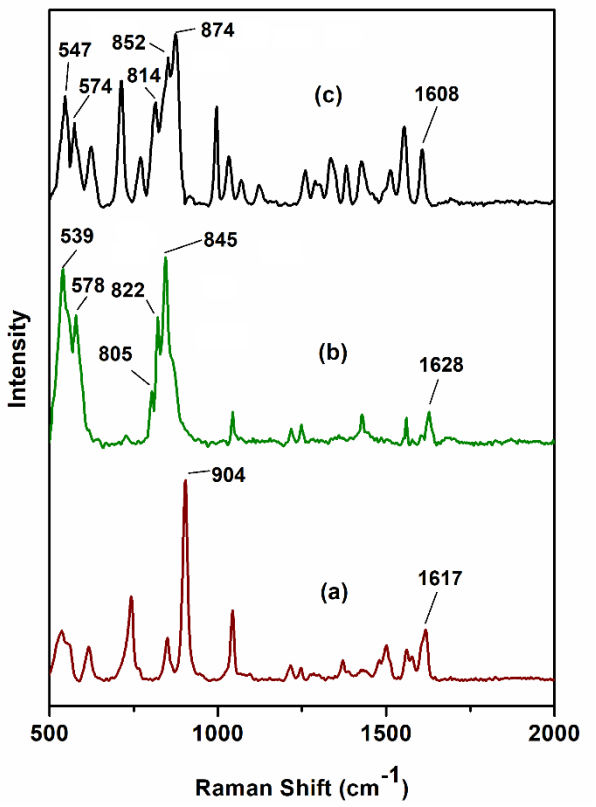

Fig. 6.3 Raman spectra of complexes (a) **6.1**, (b) **6.2** and (c) **6.3**.

6.3.2.2 Electronic spectral analysis

The UV-Visible spectra of complexes **6.1-6.3**, recorded in the aqueous solution (**Fig. 6.4**), exhibited a nearly similar spectral pattern in the 200-300 nm region. The complexes displayed two distinct bands between 200-300 nm (ε_{max}: 10,600-40,000 M^{-1} cm^{-1}) attributable to the intra-ligand π-π* and n-π* transitions in the constituent chromophores of the ligands (maltol and deferiprone) present in the complexes [65,66]. The electronic spectra of the peroxidoNb complexes **6.2** and **6.3**, recorded at a relatively higher concentration, showed an additional broad band with maxima at *ca*. 350 nm [**Fig. 6.4** (b,c) (inset)], which correspond to the peroxido to metal transition (LMCT) in the complexes [67,68].

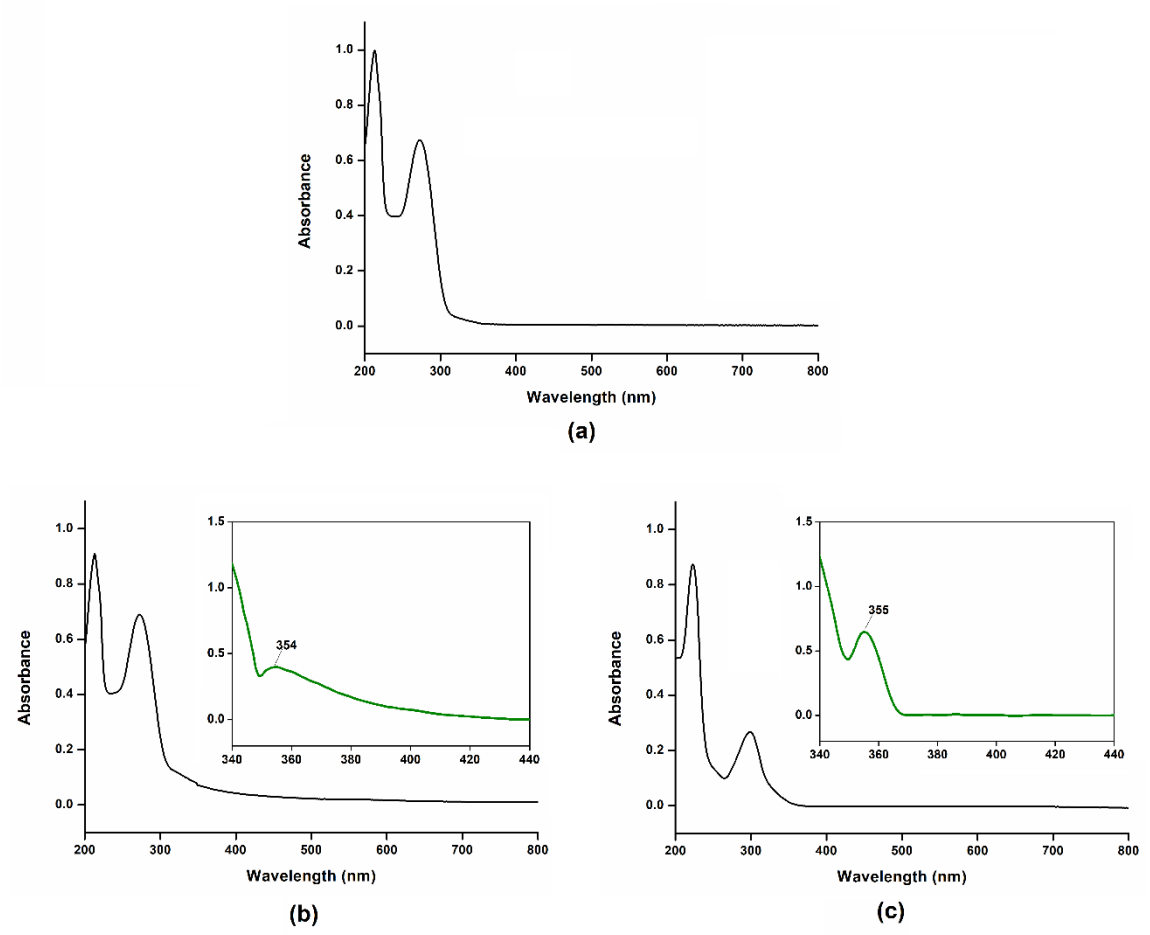

Fig. 6.4 UV–Vis absorption spectra of (a) **6.1** (conc.: 2.5 × 10^{-5} M), (b) **6.2** (conc.: 2.5 × 10^{-5} M; Inset conc.: 2.0 × 10^{-2} M) and (b) **6.3** (conc.: 2.5 × 10^{-5} M; Inset conc.: 2.0 × 10^{-2} M) in H_2O.

6.3.2.3 ^{1}H and ^{13}C NMR analysis

The ^{1}H and ^{13}C NMR spectra of complex **6.1** were recorded in methanol-d_4, whereas spectra of **6.2** and **6.3** were recorded in D_2O (**Fig. 6.5-6.10**). In **Table 6.3**, the relevant ^{1}H and ^{13}C NMR chemical shifts for the compounds as well as the free ligands, are listed for comparison. Peaks were assigned based on the available literature data [40,60,69,70]. The ^{1}H NMR spectrum of free maltol shows resonances at *ca*. 6.4, 7.6 and 2.4 ppm due to H-5, H-6 and the proton of -CH_3 group attached to C-2, respectively [60]. Considerable downfield shift of the H-5 and H-6 protons in complexes **6.1** and **6.2** relative to the free ligand values suggested the participation of the carbonyl group at C-4 in metal coordination [40,60]. Such downfield shifts are common in the case of many of the reported maltolato complexes [32,40,60,71,72]. Similar downfield shifts of the H-5 and

Table 6.3: ^{1}H and ^{13}C NMR chemical shifts for free ligands and niobium(V) complexes **6.1-6.3**

Compound	Chemical Shift (ppm)										
	^{1}H NMR				^{13}C NMR						
	H-5	H-6	CH_3(N)	CH_3(C-2)	C-2	C-3	C-4	C-5	C-6	CH_3(N)	CH_3(C-2)
Maltol	6.39	7.63	-	2.37	148.90	142.60	172.10	113.20	154.30	-	13.80
6.1	6.47	8.02	-	2.44	149.73	155.11	179.38	114.01	152.26	-	14.19
6.2	6.55	8.03	-	2.42	149.37	155.96	178.40	113.40	152.47	-	13.94
Deferiprone	6.54	7.63	3.81	2.47	141.77	147.21	171.40	114.94	138.33	44.97	14.61
6.3	6.66	7.79	3.93	2.56	141.54	154.51	178.35	114.27	138.30	44.02	13.95

[a]See **Fig. 6.12** for atom numbering

H-6 proton signals were also observed in the ^{1}H NMR spectrum of the deferiprone bonded pNb complex **6.3** as anticipated from the binding of the metal with the oxygen of the carbonyl group (C-4) during complexation.

The ^{13}C NMR spectra of both the maltol coordinated complexes **6.1** and **6.2** as well as the deferiprone containing complex **6.3**, displayed significant downfield shifts in the C-3 and C-4 carbon signals *vis-à-vis* the resonances observed in the free ligand spectra [40,60,62,69]. The observation is attributable to the chelation of the respective ligand to Nb *via* the carbonyl group at C-4 and the deprotonated hydroxyl group linked to C-3 in each of these complexes [40,62]. Thus, the ^{1}H and ^{13}C NMR spectral analysis provided unambiguous evidence in support of the successful formation of the metal complexes.

6.3.2.4 Thermogravimetric analysis

The synthesized complexes undergo multistage breakdown when the temperature is raised up to 700 ºC, as depicted in **Fig. 6.11** and **Table 6.4**. Complex **6.1** showed the first stage of decomposition within 35 to 120 ºC with a weight loss of 14.4% which is close to the calculated value of 14.3% resulting from the elimination of nine water molecules present per formula unit of the crystal. The three coordinated maltol ligands were degraded within the range of 135-550 °C by leaving the final residue of 23% as the oxidoniobium(V) species (**Table 6.4**).

The thermograms of the peroxido-Nb(V) complexes **6.2** and **6.3** showed the initial degradation within the range of 35-102 ºC due to the loss of outer sphere water molecules. The equivalent weight loss of 5.1 and 9.1% are in accordance with the values of 4.8 and 8.8% calculated for one and two molecules of water of crystallization in complexes **6.2** and **6.3**, respectively. The next step of degradation occurred in the temperature ranging from 112 to 212 ºC with the corresponding weight loss of 19.7 and 18.4% in **6.2** and **6.3**, respectively, resulting from the removal of metal-bound peroxido groups. The organic ligands, maltol or deferiprone, were released from the complexes in the subsequent step of decomposition taking place within 215-430 ºC. The residue after complete degradation of the lattice water molecules, coordinated peroxido ligands, and co-ligands of the complexes **6.2** and **6.3** were found to be 45.0 and 44.6%, respectively. The FTIR spectra of the final residues were devoid of the characteristic peaks of peroxido as well as co-ligands and showed the signature ν(Nb=O) bands of oxidoniobate species.

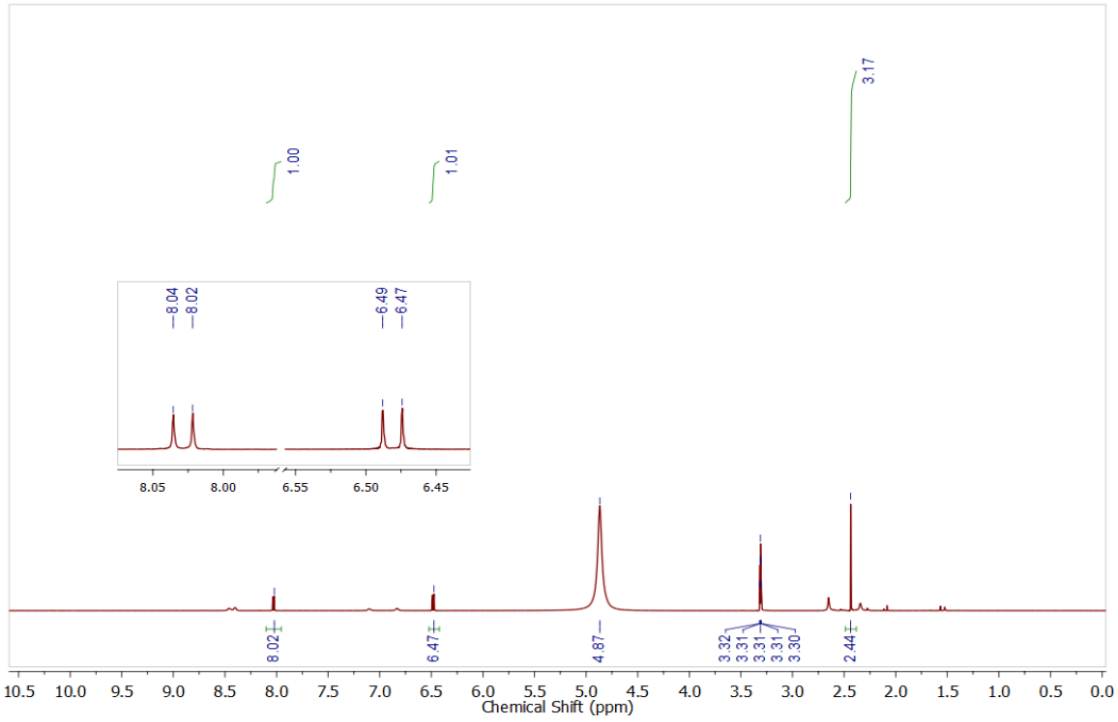

Fig. 6.5 ^{1}H NMR spectrum of **6.1** in Methanol-d_4.

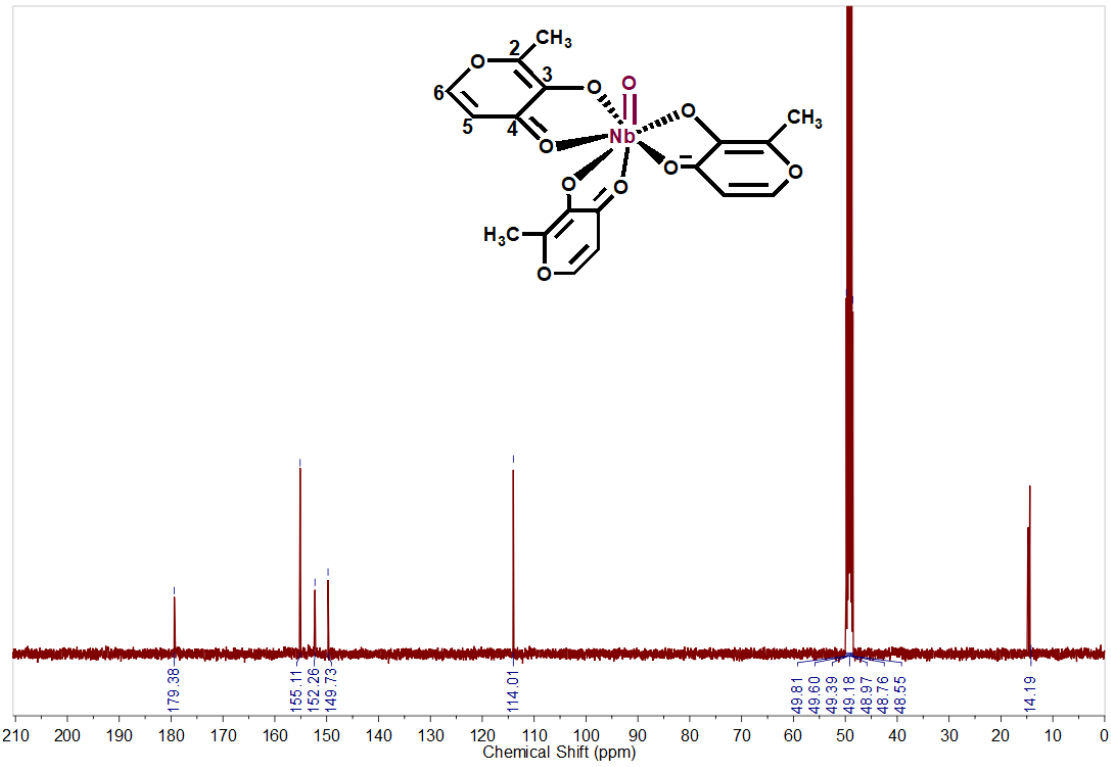

Fig. 6.6 ^{13}C NMR spectrum of **6.1** in Methanol-d_4.

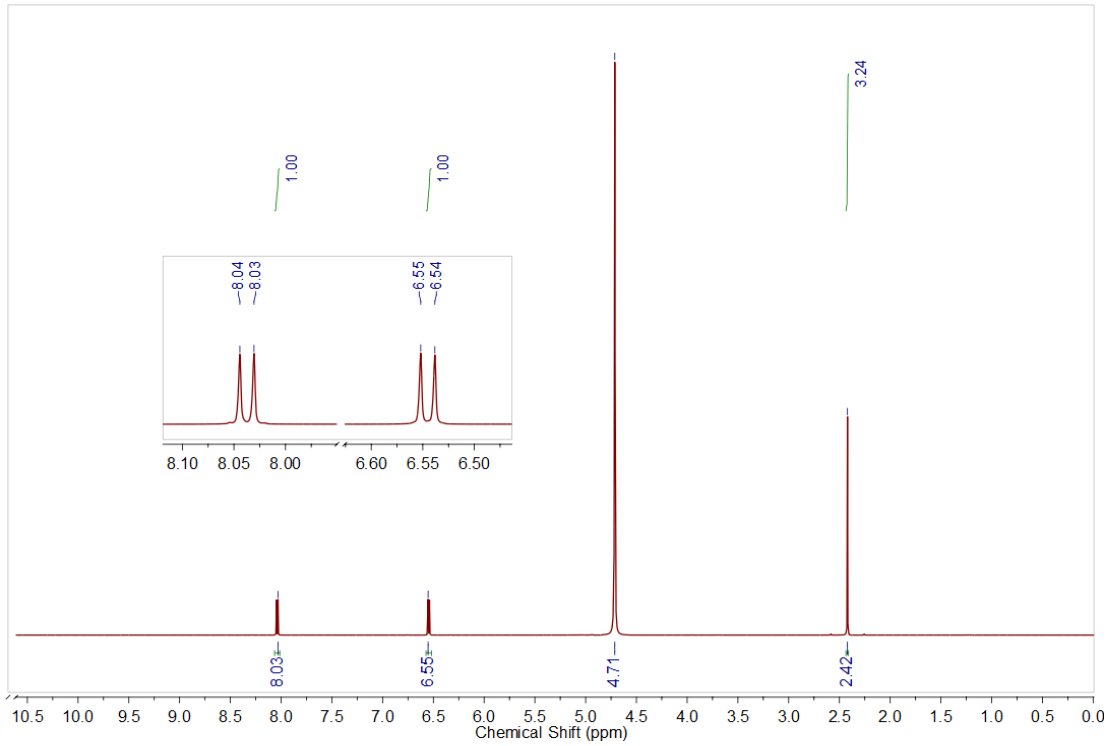

Fig. 6.7 ^{1}H NMR spectrum of **6.2** in D_2O.

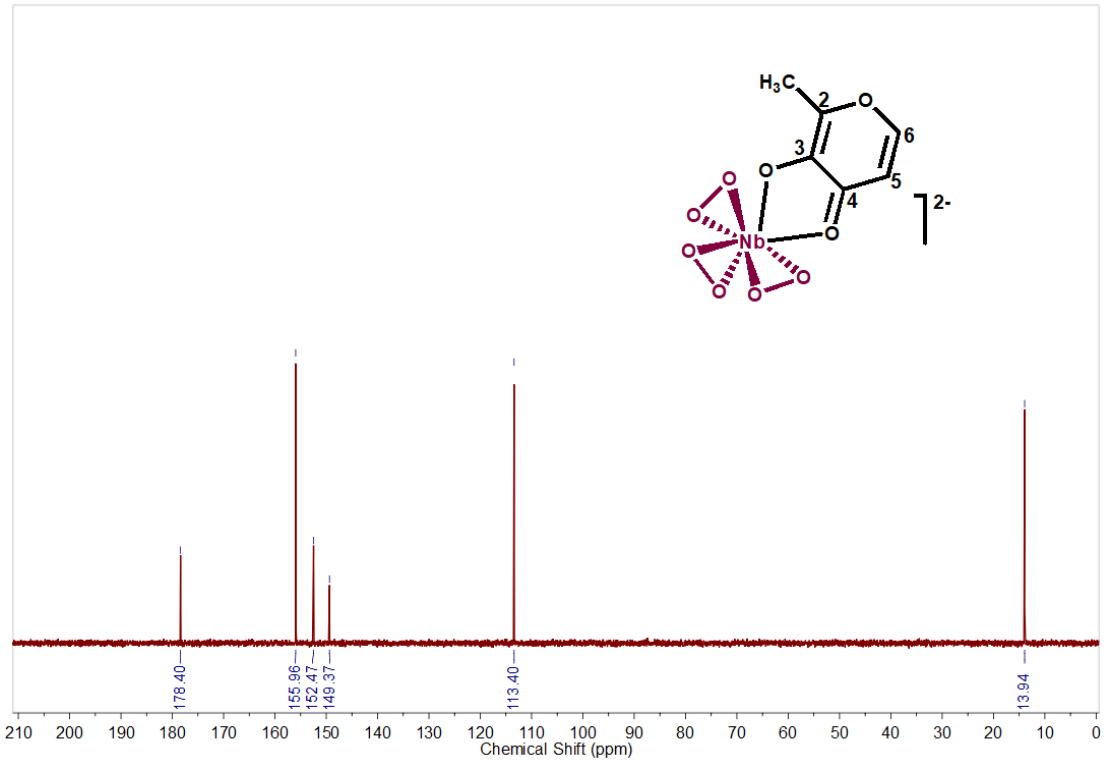

Fig. 6.8 ^{13}C NMR spectrum of **6.2** in D_2O.

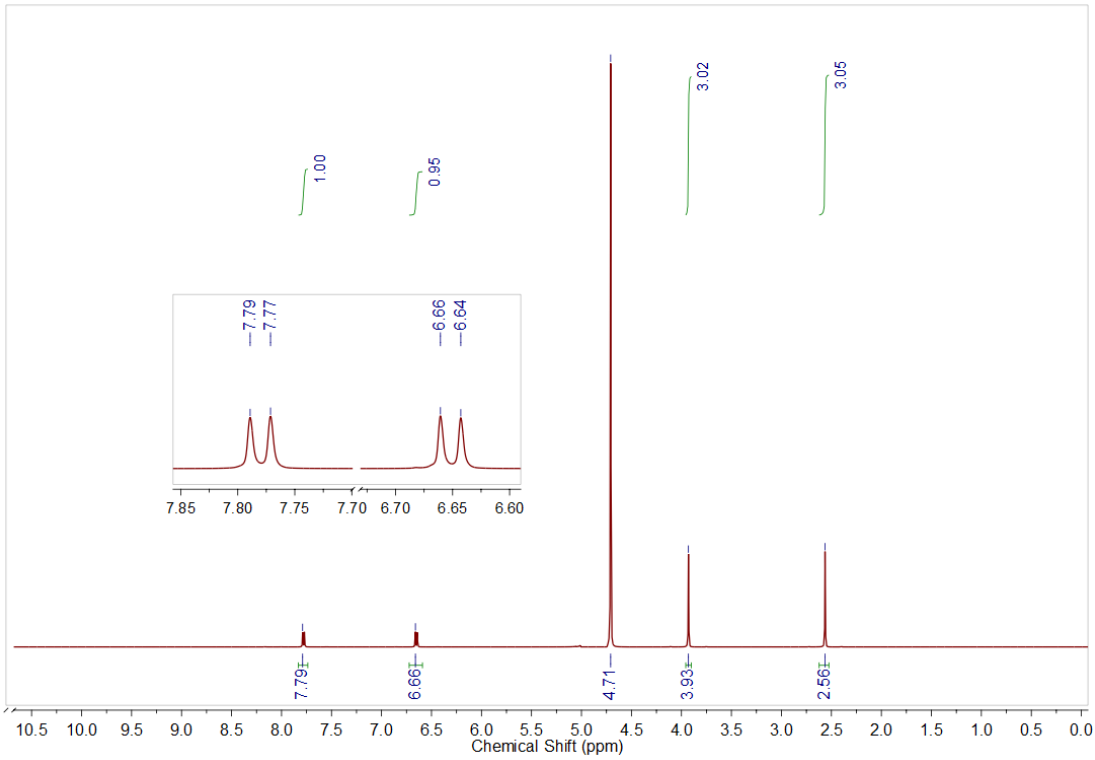

Fig. 6.9 ^{1}H NMR spectrum of **6.3** in D_2O.

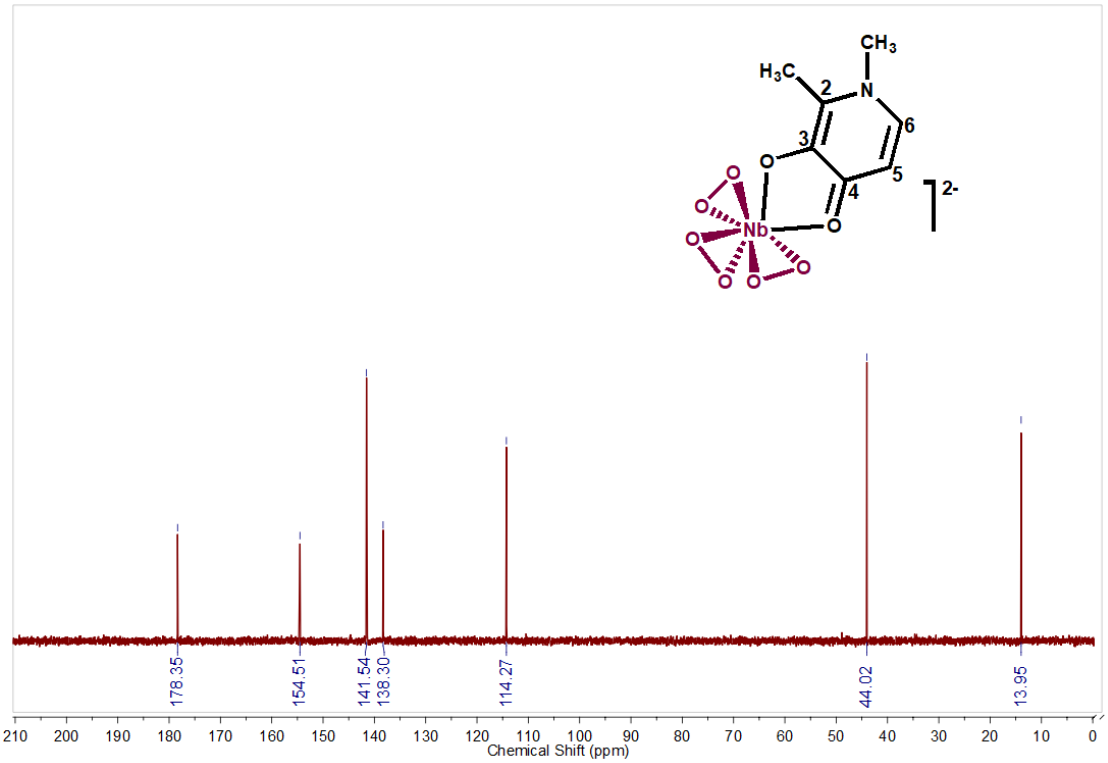

Fig. 6.10 ^{13}C NMR spectrum of **6.3** in D_2O.

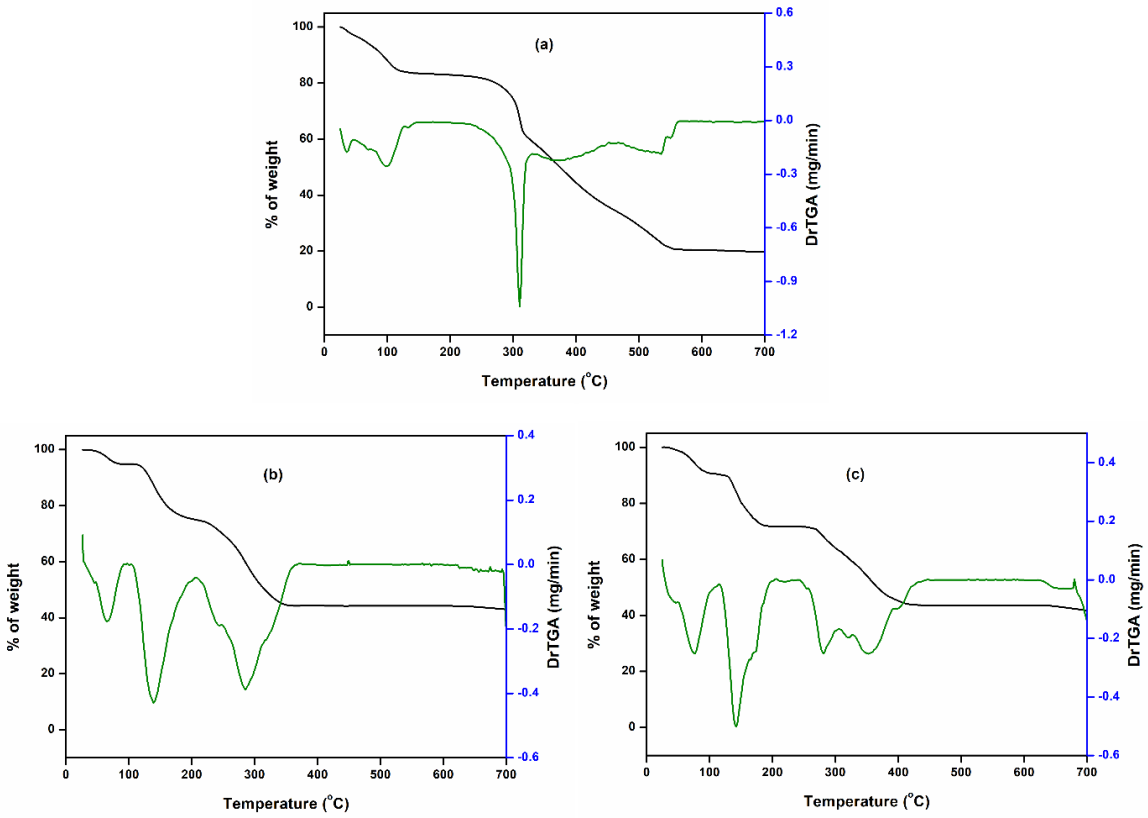

Fig. 6.11 TGA-DTG plots of (a) **6.1**, (b) **6.2** and (c) **6.3**.

Table 6.4: Thermogravimetric data of niobium(V) complexes

Compound	Temperature range (°C)	Observed weight loss (%)	Final residue (%)
6.1	35-120	14.43	23.02
	135-550	62.55	
6.2	36-102	5.07	45.01
	112-204	19.66	
	215-373	30.26	
6.3	35-102	9.10	44.56
	118-212	18.42	
	223-430	27.92	

Taking into account all the evidence gathered, the structures of the triperoxidoniobium(V) complex ions are proposed and represented in **Fig. 6.12** (a,b). Both the complex anions possess three terminal peroxido moieties and a chelating co-ligand (maltol or deferiprone) attached to Nb(V), completing the eight coordinated polyhedral geometry. The neutral oxidoniobium(V) complex $[NbO(malt)_3]_2$ exhibited a seven-

coordinated distorted pentagonal bipyramidal geometry with one oxo ligand and three chelating maltol ligands attached to the Nb(V) center [**Fig. 6.12** (c)].

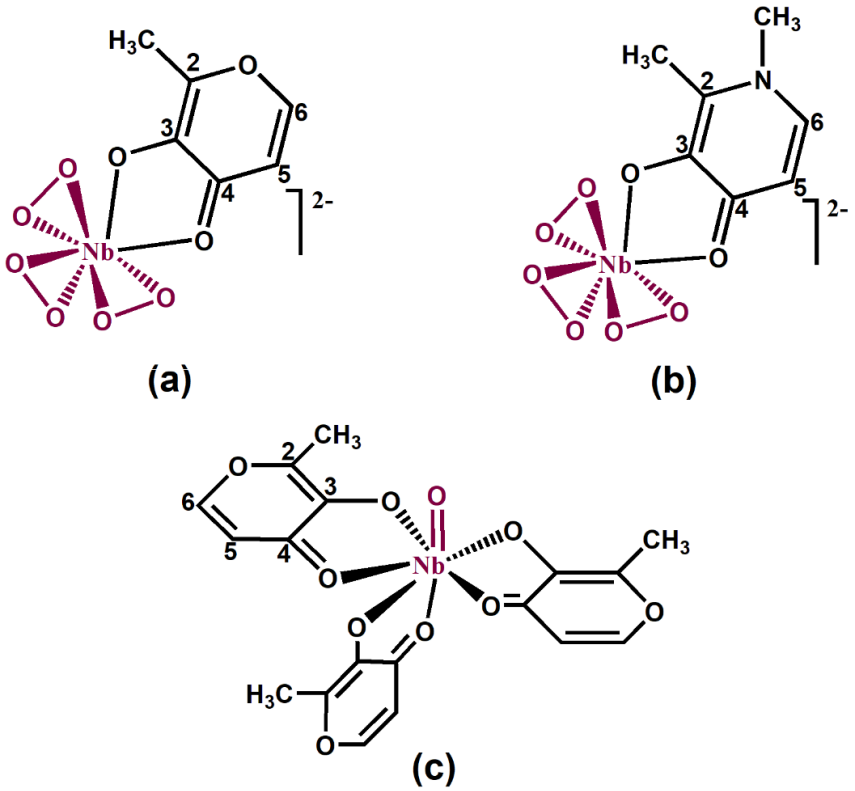

Fig. 6.12 Proposed structures of (a) **6.2** and (b) **6.3**; structure of (c) **6.1** in the current study.

6.3.3 Description of the crystal structures

The molecular structure of the oxidoniobium(V) complex $[NbO(malt)_3]_2 \cdot 9H_2O$ (**6.1**) and the corresponding bonding parameters are presented in **Fig. 6.13** and **Table 6.5**, respectively. The complex exhibited a seven-coordinated distorted pentagonal bipyramidal geometry with one oxo atom (O10) occupying the axial position, two maltol ligands occupying four equatorial coordination sites, and the third maltol ligand occupying an axial and an equatorial site (**Fig. 6.13**). All the three maltol ligands are coordinated to the niobium(V) center *via* their respective O atoms (O1 and O2; O3 and O4; O5 and O6). The Nb=O bond distance in the complex [Nb-O10 = 1.724(3) Å] (**Table 6.5**) is in the range typically observed in the reported oxidoniobium(V) complexes [63,73]. The significant distortion in the complex was quantified by the deviation of the angles O10-Nb1-O1=166.80(14)° and O10-Nb1-O4=102.46(14)° from the characteristic 180 and 90° angles of an ideal pentagonal bipyramidal geometry. The complex occurs along with four and a half water molecules (O11, O12, O13, O14, O15) as the solvent of crystallization,

out of which O14 is with 50% occupancy and shared between two similar complex moieties. The potential H-bonds exhibited by the constituent atoms of the complex are tabulated in **Table 6.6**. The H-atoms of the attached water molecules could not be allocated due to the presence of heavier metal and high degree of thermal disorder in water oxygens. As shown in **Fig. 6.14**, the water molecules (O11 and O15) present in the outer coordination sphere of the complex, form chains of H-bonding and connect two adjacent moieties through their oxo atoms (O10).

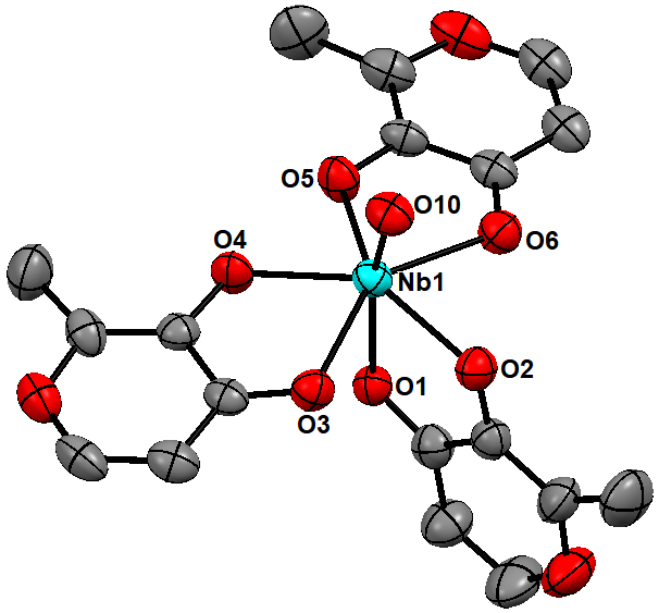

Fig. 6.13 ORTEP representation of $[NbO(malt)_3]_2 \cdot 9H_2O$ with 50% ellipsoid probability**.** The outer coordination sphere water molecules are excluded for clarity.

Table 6.5: Selected bond lengths (Å) and bond angles (º) of $[NbO(malt)_3]_2 \cdot 9H_2O$ (**6.1**)

Bond length (Å)		**Bond angle (º)**	
Nb1-O10	1.724(3)	O10-Nb1-O1	166.80(14)
Nb1-O1	2.270(3)	O10-Nb1-O2	92.98(15)
Nb1-O2	2.079(3)	O10 Nb1 O3	91.19(12)
Nb1-O3	2.223(3)	O10-Nb1-O4	102.46(14)
Nb1-O4	2.078(3)	O10-Nb1-O5	101.28(14)
Nb1-O5	2.077(3)	O10-Nb1-O6	93.86(12)
Nb1-O6	2.223(3)	O2-Nb1-O1	73.98(12)

Table 6.6: Potential hydrogen bonds in the complex $[NbO(malt)_3]_2 \cdot 9H_2O$ (**6.1**)

Entry	Donor–H···Acceptor	H···A (Å)	D–H···A (º)
1	$C_4–H_4···O_1$	2.52	130
2	$C_4–H_4···O_{10}$	2.58	131
3	$C_5–H_5···O_{10}$	2.51	133
4	$C_{16}–H_{16}···O_{11}$	2.59	179

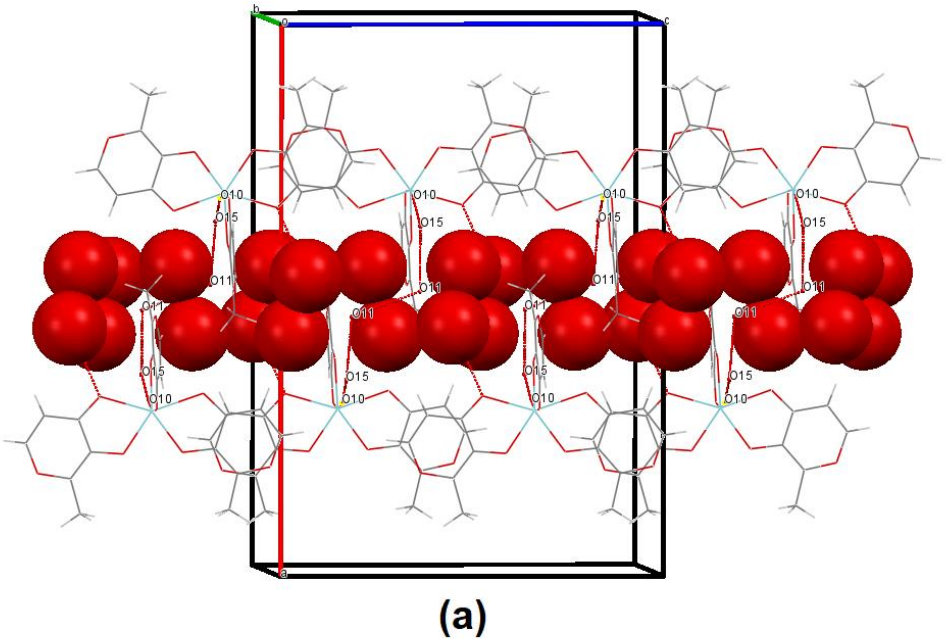

Fig. 6.14 (a), (b) Water tap through O–H···O hydrogen bonding along the crystallographic axis [001] connecting the host molecules in $[NbO(malt)_3]_2 \cdot 9H_2O$ (**6.1**).

6.3.4 Theoretical Investigation

In order to establish the viability of the structures envisaged for the pNb complexes $Na_2[Nb(O_2)_3(malt)]\cdot H_2O$ (**6.2**) and $Na_2[Nb(O_2)_3(def)]\cdot 2H_2O$ (**6.3**), we have carried out a theoretical investigation using Density Functional Theory (DFT) calculations. Presented in **Fig. 6.15** are the optimized structures of ground state geometries of the two complexes, which show the coordination spheres around the central atom. Each of the heteroleptic pNb complexes **6.2** and **6.3** possesses three peroxido groups and a co-ligand (maltol or deferiprone) coordinated to the niobium center *via* its oxygen atoms belonging to deprotonated -OH and chelating -C=O groups. In accordance with most of the reported structures of pNb complexes [4,67], both the triperoxido complexes display dodecahedral geometry around the Nb atom, where two peroxido groups are in *cis* configuration to each other, and the remaining peroxido group is in a *trans* position to the auxiliary ligand. Listed in **Table 6.7** are the selected geometrical parameters obtained from DFT calculations. It has been observed that the theoretically calculated bond lengths and bond angles of the complexes concurred well with the crystallographic parameters corresponding to previously reported mixed-ligand peroxidoniobium complexes with O-donor co-ligands in the coordination sphere [4,46,67,74-76]. Thus, the findings of our theoretical study lend credibility to the geometries proposed for the complexes **6.2** and **6.3**.

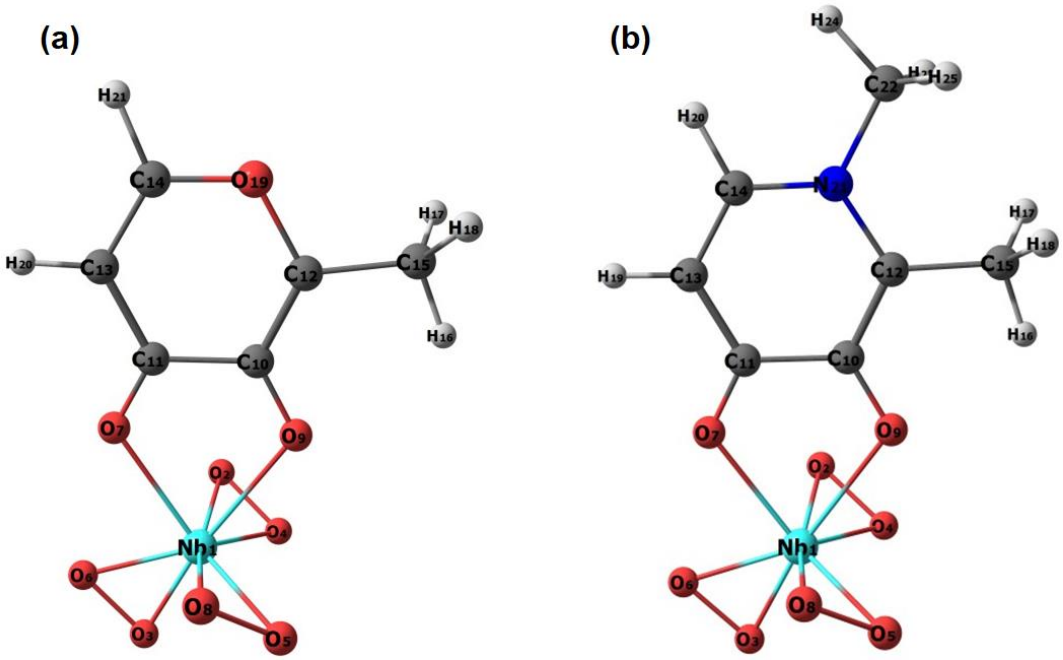

Fig. 6.15 Optimized structures of ground state geometries of the complexes (a) **6.2** and (b) **6.3** obtained at the M06-2X/def2-TZVPP level of theory.

Table 6.7: Bond lengths (Å) and bond angles (º) of the pNb complexes (a) **6.2** and (b) **6.3** corresponding to the central metal atom Nb connected to the surrounding oxygen atoms of the ligands obtained at the M06-2X/def2-TZVPP level of theory

Structural index[a]	6.2	6.3
Nb1-O2	1.97945	1.98143
Nb1-O3	1.94981	1.95288
Nb1-O4	1.97663	1.98113
Nb1-O5	1.97664	1.97905
Nb1-O6	1.98068	1.97953
Nb1-O7	2.34255	2.31100
Nb1-O8	1.97946	1.98057
Nb1-O9	2.41861	2.42149
O2-O4	1.46055	1.46020
O5-O8	1.46054	1.46089
O3-O6	1.45903	1.45921
∠O3-Nb1-O6	43.572	43.557
∠O2-Nb1-O4	43.331	43.246
∠O5-Nb1-O8	43.331	43.301
∠O7-Nb1-O9	68.358	68.436

See **Fig. 6.15** for atom numbering

6.3.5 Stability of the compounds in aqueous solution

Prior to exploring their enzyme inhibitory potential, we considered it imperative to ascertain the stability of the complexes **6.1-6.3** in aqueous solution under varying pH conditions. In the present study, as evidenced by ^{1}H and ^{13}C NMR, as well as UV-Vis spectroscopic analysis (**Fig. 6.16-6.18**), each of the compounds examined, remain stable in aqueous solution for at least up to a period of 12 h. These observations are indeed significant, considering that the bis(maltolato)oxidovanadium (BMOV) complex was reported to undergo ready dissociation in an aqueous solution [42,44,77]. In the case of the peroxidoniobium complexes, it was further observed that the peroxide content of all the compounds under investigation, including the macromolecular complex **NbPMA** (**4.1**), remained virtually unchanged over a span of 12 h. The stability of the pNb

complexes was also assessed in the solution of pH values 8.0, 7.0 and 4.6**.** It is remarkable that, as revealed by our study, these compounds remained intact in this wide range of pH values including at acidic pH.

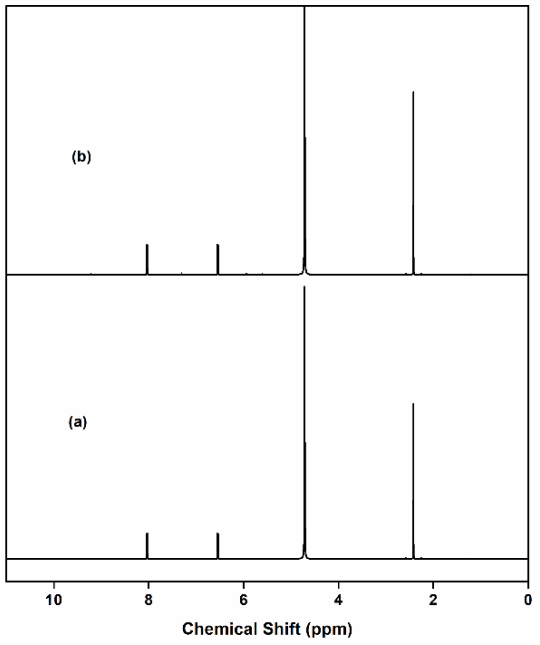

Fig. 6.16 ^{1}H NMR spectra of complex **6.2** in D_2O. The spectra were recorded as follows: (a) solution of complex **6.2** instantly after preparation and (b) solution of (a) after 12 h.

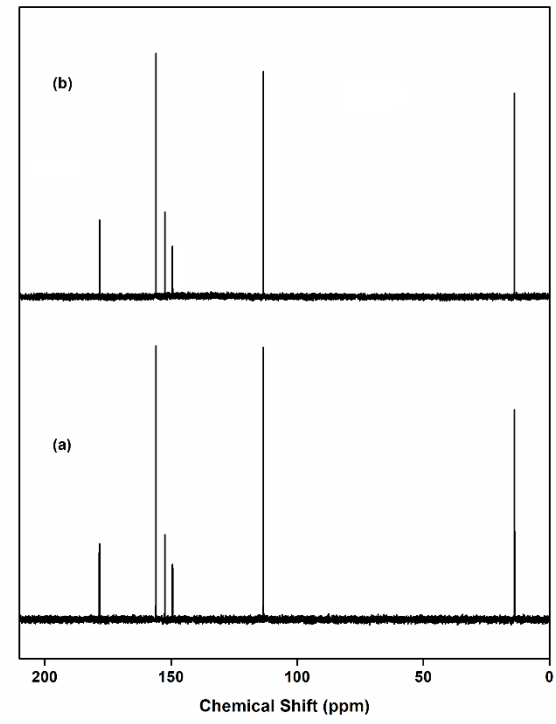

Fig. 6.17 ^{13}C NMR spectra of the complex **6.2** in D_2O. The spectra were recorded as follows: (a) solution of **6.2** instantly after preparation and (b) solution of (a) after 12 h.

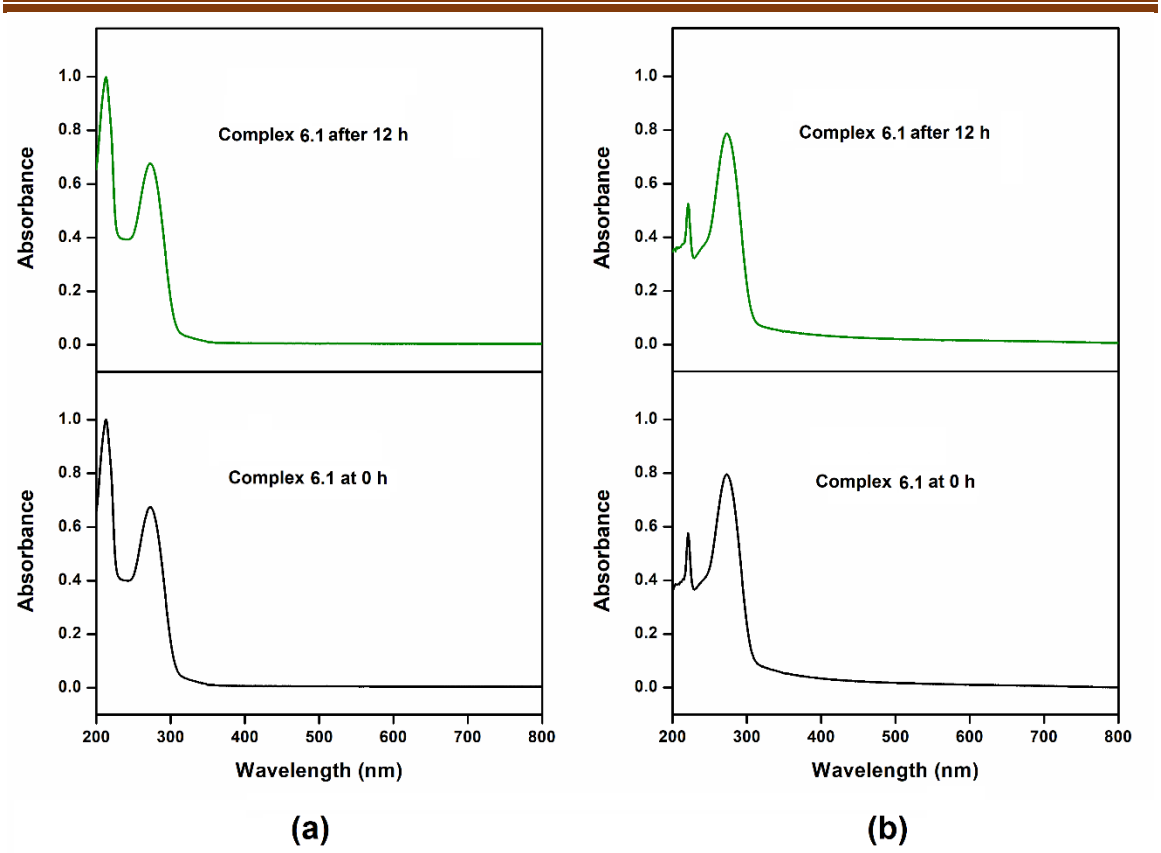

Fig. 6.18 UV-visible spectra of complex **6.1** recorded immediately after preparation and 12 h later (a) at natural pH (5.2) of the complex and (b) at pH = 4.6.

6.3.6 Nb(V) compounds as phosphatase inhibitors

Inhibition of wheat thylakoid membrane ACP-catalyzed dephosphorylation of *para*-nitrophenyl phosphate (*p*-NPP) by the niobium(V) complexes **4.1**, **6.1-6.3** was examined *in vitro* using a standard enzyme assay system. We have chosen acid phosphatases for our study as this class of enzymes has often been considered as useful models for investigating metal-induced inhibition in membrane proteins [53,78,79].

The concentration-dependent inhibition of the function of ACP with respect to the substrate *p*-NPP by the investigated Nb(V) complexes presented in **Fig. 6.19** demonstrates that, % ACP activity gradually decreased with increasing dose of each of the tested compounds. The IC_{50} values (half-maximal inhibitory concentration) obtained from these plots enabled us to measure quantitatively the inhibitory efficiency of each of the species. The IC_{50} values for the inhibitors varying within the micromolar range (**Fig. 6.19** and **Table 6.8**) demonstrate that each of the Nb(V) complexes is an effective inhibitor of ACP, irrespective of the nature of their ligand environment. On the other hand, the variation of

IC_{50} values within a wide range of 6-64 μM indicated that variation in the organic ligand has a distinct impact on the inhibitor potency of the complexes. The oxidoniobium(V)maltol complex **6.1** was observed to be a relatively weaker inhibitor in comparison to the peroxidoniobium(V) complexes, whereas the **PMA**-supported compound **4.1**, with its IC_{50} value as low as 6.59 μM found to be most efficient among the range of compounds studied. Interestingly, a somewhat similar trend was observed during our previous investigations on phosphatase inhibition by free monomeric and polymer-anchored peroxido complexes of V, Mo, and W [25,28,30]. Importantly, the free ligands maltol, deferiprone or the polymers alone did not induce any observable effect on the activity of the enzyme, under the applied assay condition.

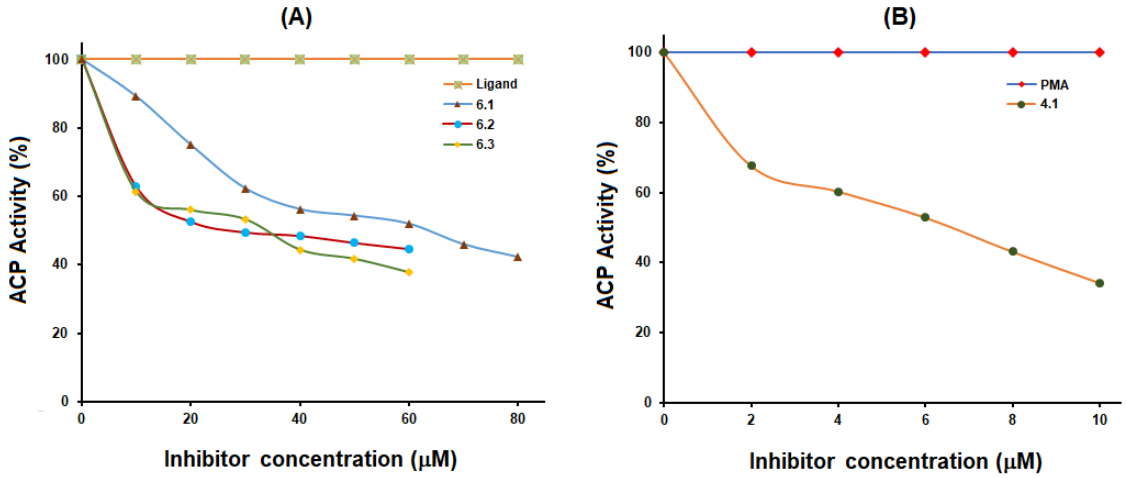

Fig. 6.19 The effect of Nb(V) complexes and free ligands on ACP catalyzed rates of hydrolysis of *p*-NPP at pH 4.6 at stated concentrations of inhibitors. (A) For **6.1** and the free ligand maltol, concentrations are: 10, 20, 30, 40, 50, 60, 70 and 80 μM and for **6.2**, **6.3** and free ligand deferiprone, compound concentrations: 10, 20, 30, 40, 50 and 60 μM, (B) for **NbPMA** (**4.1**) and free ligand poly(sodium methacrylate) (**PMA**), compound concentrations: 2, 4, 6, 8 and 10 μM. The results are expressed as means ±SE (n = 3). The concentrations of the polymeric compound are based on actual niobium loading.

6.3.7 Kinetics of ACP inhibition by the Nb(V) complexes

The activity of an enzyme can be inhibited by an inhibitor species *via* various pathways such as competitive, uncompetitive, non-competitive or mixed inhibition. As revealed by the relevant literature, in order to distinguish among different mechanisms of inhibition, enzyme kinetic investigation has been recognized as a highly useful tool [54,57-

59,80-82]. Accordingly, with an aim to gain an insight into the mode of the inhibition of ACP activity by the Nb(V) complexes, the steady-state kinetics of inhibition were investigated. The kinetic parameters, K_m and V_{max}, were measured from the Lineweaver-Burk (L-B) double reciprocal plots [54,57-59,80]. The L-B plots of 1/v against 1/[S] in the presence of variable concentrations of inhibitors are presented in **Fig. 6.20**. The resulting data for the neat monomeric peroxido niobium complexes yielded straight lines with a point of intersection in the second quadrant [**Fig. 6.20** (A, B)]. In each case, an increase in [I] (inhibitor concentration) led to an enhancement of the K_m value, whereas the value of V_{max} diminished. The observations signified that these complexes are mixed competitive and non-competitive inhibitors of ACP [44,57,58]. On the other hand, in the case of the macromolecular pNb complexes as well as the oxidoniobium complex [**Fig. 6.20** (C, D)], L-B plots revealed that K_m remained unchanged with increasing dose of inhibitor although a decrease in velocity, V_{max} occurred. Thus, the observed pattern is typical of a non-competitive mode of inhibition [57-59].

As can be seen in the inset to **Fig. 6.20**, the inhibitor constant K_i, which represents the affinity of the inhibitor towards the free enzyme [57,58,80,81], was determined from the secondary plot of the slope of these lines versus the concentration of inhibitor where the *x*-intercept was defined as $-K_i$. The value of K_{ii}, the inhibitor constant representing the inhibitor's affinity of the enzyme-substrate complex (ACP-*p*NPP), was found from the secondary plot of the intercepts of the primary L-B plot against [I]. The results obtained for all the monomeric pNb complexes (**Table 6.8**) showed that $K_{ii} > K_i$, which is characteristic of a mixed type of inhibition [44,58,82]. On the contrary, for the polymer anchored complex **4.1** [**Fig. 6.20** (D), **Table 6.8**] and also for the oxidoniobium complex **6.1** [**Fig. 6.20** (C), **Table 6.8**] the ratio obtained for K_{ii}/K_i being near to unity with comparable values of the inhibitor constants K_i and K_{ii}, signified that these complexes are non-competitive inhibitors of ACP [58,59,81,82].

A non-competitive inhibitor usually influences enzyme activity by altering the overall three-dimensional conformation of the enzyme as it binds reversibly at a site distant from the active site of the enzyme [11,59,81,83]. On the other hand, competitive inhibitors display a close structural analogy to the natural substrate of the enzyme [18,57,58]. Due to the structural similarity with the phosphate group, relatively smaller oxy-anions of V, Mo and W with penta- or hexa-coordinated geometries generally inhibit phosphatases in a competitive manner [17,18,84-86]. In regard to the inhibition of ACP, however, different

oxidometallates have been reported to show diverse mechanistic preferences, *viz*., competitive, non-competitive or uncompetitive inhibition [17,18,84-88]. In the present study, the non-competitive mode of inhibition observed in case of tris(maltolato)oxidoniobium(V) complex is indeed significant considering that the corresponding vanadium complex BMOV was reported to perform as a competitive inhibitor of ALP whereas, in the case of protein tyrosine phosphatase (GST-PTP1B) it acted as a mixed competitive and non-competitive type inhibitor [44]. Some earlier kinetic data also showed that BMOV inhibition, in effect, resembled the inhibition mode exerted by orthovanadate due to the fact that BMOV dissociates in an aqueous solution into vanadate, and maltol plays no role in inhibition [44,77]. In contrast, tris(maltolato)oxidoniobium(V) (**6.1**) has been observed to retain its structure in the aqueous solution of a wide range of pH values. Our results thus clearly indicated that the observed non-competitive inhibition of complex **6.1** originates from the interaction of the intact complex with the enzyme. As a consequence of the presence of relatively bulkier maltol ligands in its coordination sphere, it is unlikely to approach the enzyme active site to function as a competitive inhibitor.

Several previous studies dealing with phosphatase inhibition by vanadium compounds have demonstrated that apart from the nature of the enzyme, factors like metal oxidation state, coordination geometry and structural integrity of the compounds under physiological conditions may be responsible for deciding the inhibitor potency as well as the mode of inhibition of the phosphohydrolases [11,15,17]. Acid phosphatases, extracted from a variety of plant and animal sources such as wheat germ and human prostate, possess an active site containing dinuclear Fe^{2+} bound to a histidine residue and highly conserved sequences of amino acids [53,83,89-91]. Active oxidative species have been shown to inhibit thylakoid ACP function in a non-competitive manner *via* oxidative interaction leading to the oxidative transformation of the active site Fe^{2+} to Fe^{3+} form [83]. In this context, it is relevant to recall previous findings from our laboratory, which has successfully established that polymer-anchored macromolecular peroxido complexes of a range of d^0 metal ions, including V, Mo and W, inhibited the function of phosphatases such as ALP and ACP in a non-competitive manner, whereas their low molecular weight monomeric congeners usually induced mixed type of inhibition on these enzyme functions [25,28,29]. Thus, results of our present study with respect to ACP inhibition, validate our earlier findings.

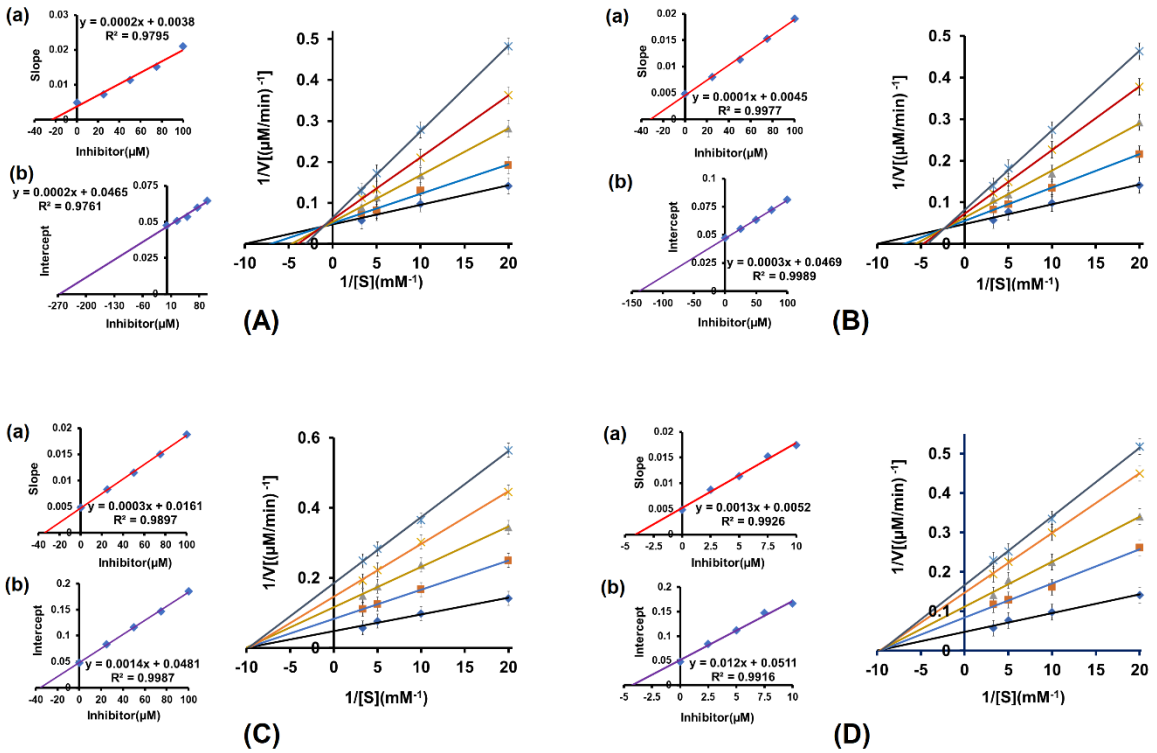

Fig. 6.20 L-B plots for the ACP inhibition in the absence and presence of ♦ 0 μM, ■ 25μM, ▲ 50 μM, X 75 μM, ж 100 μM concentrations of (A) **6.2**, (B) **6.3,** (C) **6.1** and (**D**) ♦ 0 μM, ■ 2.5μM, ▲ 5 μM, X 7.5 μM, ж 10 μM concentrations of **NbPMA** (**4.1**). The reaction started with the addition of ACP (18.38 μg mL^{-1}) to the pre-incubated reaction solution of 0.1 M acetate buffer (pH 4.6) and *p*-NPP (50-300 μM) and then the rates of hydrolysis were determined. The results are expressed as means ±SE (n =3) from independent experiments. Inset: (a) secondary plot of slopes versus [I], where *x*-intercept defines the K_i value. (b) secondary plot of *y*-intercepts against [I], where *x*-intercept refers to K_{ii} value.

There has been a number of reports available which co-related the protein phosphatase inhibition activity by pV species to its ability to oxidize the cysteine thiol group in the catalytic domain of PTPase [11,17,86]. We have surmised earlier that oxidative interaction between the cysteine-SH groups and the inhibitor species to be a likely cause of the observed non-competitive inhibition displayed by these systems [25,28]. A similar oxidative mechanism appears possible in the present study also, keeping in view that our previous work [68,92], demonstrated that various heteroleptic peroxidoniobate(V) compounds can serve as efficient stoichiometric oxidants as well as highly active catalysts in aqueous phase organic oxidations. However, due to the dearth of

direct evidence and in view of the complexity of interacting species and the biological process involved, we are constrained in drawing any further conclusion at this stage regarding the exact mechanism of the observed inhibition.

Table 6.8: The values of IC_{50} and inhibitor constants (K_i and K_{ii}) determined for ACP inhibition

Compound	IC_{50} (μM)	K_i(μM)	K_{ii}(μM)	K_{ii}/K_i	Types of inhibition
6.1	63.66	34.90	36.28	1.04	Non-competitive
6.2	26.51	24.40	263.5	10.79	Mixed inhibition
6.3	33.75	31.75	137.75	4.34	Mixed inhibition
4.1	6.59	4.05	4.14	1.02	Non-competitive

6.4 Conclusions

The present work provided an access to two new water-soluble and stable heteroleptic triperoxidoniobium(V) complexes (**6.2** and **6.3**) with maltol or deferiprone as co-ligands, as well as a neutral tris(maltolato)oxido-Nb(V) complex (**6.1**). The molecular structure of complex **6.1** has been confirmed by single crystal X-Ray diffraction studies, which revealed a distorted pentagonal bipyramidal geometry. The spectral and chemical analysis data pertaining to complexes **6.2** and **6.3** corroborated by the results of DFT calculations, furnished unambiguous evidence for the composition of the coordination sphere and likely mode of metal-ligand bonding in these complexes. It is noteworthy that each of the synthesized complexes has been observed to remain stable in the aqueous solution of a wide range of pH values, including acidic pH.

Our findings from the *in vitro* study on ACP activity convincingly demonstrated the effectiveness of niobium(V) compounds as potent inhibitors of ACP, irrespective of their being free or polymer anchored. Steady-state enzyme kinetic analysis showed that the inhibitors under investigation can be categorized into two distinct types on the basis of their mechanistic preference for inhibiting the enzyme activity. The monomeric low molecular weight pNb compounds exerted mixed type of inhibition, whereas macromolecular niobium peroxido compound acted as classical non-competitive inhibitor of ACP. It is significant to note that, relatively bulkier tris(maltolato)oxidoniobium complex **6.1** inhibited the model enzyme *via* a non-competitive pathway. Interestingly,

polymer-anchored compound is nearly 4-5 fold more potent compared to the free monomeric pNb complexes. These data are in accord with our previous observations pertaining to the inhibitory activity of peroxidovanadium and peroxidomolybdenum complexes on the function of alkaline phosphatase [25]. Overall, the findings of the present investigation have unraveled newer facets of oxido and peroxido niobium(V) systems which are interesting from chemical as well as biological perspectives.

References

1. Safavi, M. S., Walsh, F., Visai, L., and Khalil-Allafi, J. Progress in niobium oxide-containing coatings for biomedical applications: A critical review. *ACS Omega*, 7(11):9088-9107, 2022.
2. Rydzynski, K. and Pakulska, D. *Patty's Industrial Hygiene and Toxicology.* John Wiley & Sons Press, New Jersey, 2012.
3. Fraqueza, G., Ohlin, C. A., Casey, W. H., and Aureliano, M. Sarcoplasmic reticulum calcium ATPase interactions with decaniobate, decavanadate, vanadate, tungstate and molybdate. *Journal of Inorganic Biochemistry*, 107(1):82-89, 2012.
4. Bayot, D. and Devillers, M. Peroxo complexes of niobium(V) and tantalum(V). *Coordination Chemistry Reviews*, 250(19-20):2610-2626, 2006.
5. Stavber, G., Malič, B., and Kosec, M. A road to environmentally friendly materials chemistry: Low-temperature synthesis of nanosized $K_{0.5}Na_{0.5}NbO_3$ powders through peroxide intermediates in water. *Green Chemistry*, 13(5):1303-1310, 2011.
6. Pereira-Maia, E. C., Souza, I. P., Nunes, K. J., Castro, A. A., Ramalho, T. C., Steffler, F., Duarte, H. A., Pacheli, A., Chagas, P., and Oliveira, L. C. Peroxoniobium inhibits leukemia cell growth. *RSC Advances*, 8(19):10310-10313, 2018.
7. Thomadaki, H., Lymberopoulou-Karaliota, A., Maniatakou, A., and Scorilas, A. Synthesis, spectroscopic study and anticancer activity of a water-soluble Nb(V) peroxo complex. *Journal of Inorganic Biochemistry*, 105(2):155-163, 2011.
8. Maniatakou, A., Karaliota, S., Mavri, M., Raptopoulou, C., Terzis, A., and Karaliota, A. Synthesis, characterization and crystal structure of novel mononuclear peroxotungsten(VI) complexes. Insulinomimetic activity of W(VI) and Nb(V) peroxo complexes. *Journal of Inorganic Biochemistry*, 103(5):859-868, 2009.
9. Rehder, D., Bashipoor, M., Jantzen, S., Schmidt, H., Farahbakhsh M., and Nekola, H. In Tracey A. S. and D. C. Crans, D. C., editors, *Vanadium Compounds: Chemistry, Biochemistry, and Therapeutic Applications*, pages 60-71. Oxford University Press, New York, 1998.
10. Tracey, A. S., Willsky, G. R., and Takeuchi, E. S. *Vanadium: Chemistry, Biochemistry, Pharmacology and Practical Applications*. CRC press and Taylor & Francis Group, Boca Raton, 2007.

11. Aureliano, M., Gumerova, N. I., Sciortino, G., Garribba, E., McLauchlan, C. C., Rompel, A., and Crans, D. C. Polyoxidovanadates' interactions with proteins: An overview. *Coordination Chemistry Reviews*, 454:214344, 2022.
12. Ramasarma, T. The emerging redox profile of vanadium. *Proceedings of the Indian National Science Academy B*, 69(4):649-672, 2003.
13. Treviño, S. and Diaz, A. Vanadium and insulin: Partners in metabolic regulation. *Journal of Inorganic Biochemistry*, 208:111094, 2020.
14. Parente, J. E., Naso, L. G., Jori, K., Franca, C. A., da Costa Ferreira, A. M., Williams, P. A., and Ferrer, E. G. *In vitro* experiments and infrared spectroscopy analysis of acid and alkaline phosphatase inhibition by vanadium complexes. *New Journal of Chemistry*, 43(45):17603-17619, 2019.
15. Louie, A. Y., Meade, T. J., and Lippard, S. Metal complexes as enzyme inhibitors. *Chemical Reviews*, 99(9):2711-2734, 1999.
16. Feng, B., Dong, Y., Shang, B., Zhang, B., Crans, D. C., and Yang, X. Convergent protein phosphatase inhibitor design for PTP1B and TCPTP: Exchangeable vanadium coordination complexes on graphene quantum dots. *Advanced Functional Materials*, 32(5):2108645, 2022.
17. Crans, D. C., Smee, J. J., Gaidamauskas, E., and Yang, L. The chemistry and biochemistry of vanadium and the biological activities exerted by vanadium compounds. *Chemical Reviews*, 104(2):849-902, 2004.
18. McLauchlan, C. C., Peters, B. J., Willsky, G. R., and Crans, D. C. Vanadium–phosphatase complexes: Phosphatase inhibitors favor the trigonal bipyramidal transition state geometries. *Coordination Chemistry Reviews*, 301:163-199, 2015.
19. Hunter, T. Signaling—2000 and beyond. *Cell*, 100(1):113-127, 2000.
20. Haldar, A. K., Banerjee, S., Naskar, K., Kalita, D., Islam, N. S., and Roy, S. Sub-optimal dose of sodium antimony gluconate (SAG)-diperoxovanadate combination clears organ parasites from BALB/c mice infected with antimony resistant Leishmania donovani by expanding antileishmanial T-cell repertoire and increasing IFN-γ to IL-10 ratio. *Experimental Parasitology*, 122(2):145-154, 2009.
21. Chatterjee, N., Kiran, S., Ram, B. M., Islam, N. S., Ramasarma, T., and Ramakrishna, G. Diperoxovanadate can substitute for H_2O_2 at much lower concentration in inducing features of premature cellular senescence in mouse fibroblasts (NIH3T3). *Mechanisms of Ageing Development*, 132(5):230-239, 2011.

22. Khanna, V., Jain, M., Barthwal, M. K., Kalita, D., Boruah, J. J., Das, S. P., Islam, N. S., Ramasarma, T., and Dikshit, M. Vasomodulatory effect of novel peroxovanadate compounds on rat aorta: role of rho kinase and nitric oxide/cGMP pathway. *Pharmacological Research*, 64(3):274-282, 2011.
23. Chatterjee, N., Anwar, T., Islam, N. S., Ramasarma, T., and Ramakrishna, G. Erratum to: Growth arrest of lung carcinoma cells (A549) by polyacrylate-anchored peroxovanadate by activating Rac1-NADPH oxidase signalling axis. *Molecular and Cellular Biochemistry*, 424:209-210, 2017.
24. Kalita, D., Sarmah, S., Das, S. P., Baishya, D., Patowary, A., Baruah, S., and Islam, N. S. Synthesis, characterization, reactivity and antibacterial activity of new peroxovanadium(V) complexes anchored to soluble polymers. *Reactive and Functional Polymers*, 68(4):876-890, 2008.
25. Boruah, J. J., Kalita, D., Das, S. P., Paul, S., and Islam, N. S. Polymer-anchored peroxo compounds of vanadium(V) and molybdenum(VI): Synthesis, stability, and their activities with alkaline phosphatase and catalase. *Inorganic Chemistry*, 50(17):8046-8062, 2011.
26. Hazarika, P., Kalita, D., and Islam, N. S. Mononuclear and dinuclear peroxotungsten complexes with co-ordinated dipeptides as potent inhibitors of alkaline phosphatase activity. *Journal of Enzyme Inhibition and Medicinal Chemistry*, 23(4):504-513, 2008.
27. Gogoi, S. R., Saikia, G., Ahmed, K., Duarah, R., and Islam, N. S. Niobium(V) peroxo α-amino acid complexes: Synthesis, stability and kinetics of inhibition of acid phosphatase activity. *Polyhedron*, 121:142-154, 2017.
28. Saikia, G., Talukdar, H., Ahmed, K., Gour, N. K., and Islam, N. S. Tantalum(V) peroxido complexes as phosphatase inhibitors: A comparative study *vis-à-vis* peroxidovanadates. *New Journal of Chemistry*, 45(29):12848-12862, 2021.
29. Das, S. P., Ankireddy, S. R., Boruah, J. J., and Islam, N. S. Synthesis and characterization of peroxotungsten(VI) complexes bound to water soluble macromolecules and their interaction with acid and alkaline phosphatases. *RSC Advances*, 2(18):7248-7261, 2012.
30. Saikia, G., Gogoi, S. R., Boruah, J. J., Ram, B. M., Begum, P., Ahmed, K., Sharma, M., Ramakrishna, G., Ramasarma, T., and Islam, N. S. Peroxo compounds of

vanadium(V) and niobium(V) as potent inhibitors of calcineurin activity towards RII-Phosphopeptide. *ChemistrySelect*, 2(21):5838-5848, 2017.

31. Kiran, K. R. Synthesis, characterization and antibacterial activity of Cu(II), Zn(II) ternary complexes with maltol and glycylglycine. *Chemical Science Transactions*, 3:592-601, 2014.
32. Faraglia, G., Fregona, D., and Sitran, S. Complexes of aluminum, gallium and indium with pyrone derivatives. *Main Group Metal Chemistry*, 17(9):649-658, 1994.
33. Melchior, M., Rettig, S. J., Liboiron, B. D., Thompson, K. H., Yuen, V. G., McNeill, J. H., and Orvig, C. Insulin-enhancing vanadium(III) complexes. *Inorganic Chemistry*, 40(18):4686-4690, 2001.
34. Clevette, D. J., Nelson, W. O., Nordin, A., Orvig, C., and Sjoeberg, S. The complexation of aluminum with N-substituted 3-hydroxy-4-pyridinones. *Inorganic Chemistry*, 28(11):2079-2081, 1989.
35. Mendi, F. D., Sh. Saljooghi, A., Ramezani, M., Kruszynski, R., Poupon, M., Kucerakova, M., Huch, V., Socha, P., Babaei, M., and Alibolandi, M. Five new complexes with deferiprone and N, N-donor ligands: evaluation of cytotoxicity against breast cancer MCF-7 cell line and HSA-binding determination. *Journal of Biomolecular Structure and Dynamics*, 39(13):4845-4858, 2021.
36. Nurchi, V. M., Crisponi, G., Pivetta, T., Donatoni, M., and Remelli, M. Potentiometric, spectrophotometric and calorimetric study on iron(III) and copper(II) complexes with 1, 2-dimethyl-3-hydroxy-4-pyridinone. *Journal of Inorganic Biochemistry*, 102(4), 684-692, 2008.
37. Nazari, M., Salehi, S., Moghadam, S. M. M., Babaei, M., and Saljooghi, A. Vanadium complexes with maltol and deferiprone ligands: Synthesis, characterization and in vitro antiproliferative activity toward different cancer cells. *Inorganic Chemistry Research*, 4(1):123-131, 2020.
38. Schmidt, C., Allen, S., Kopyt, N., and Pergola, P. Iron replacement therapy with oral ferric maltol: Review of the evidence and expert opinion. *Journal of Clinical Medicine*, 10(19):4448, 2021.
39. Thompson, K. H., Barta, C. A., and Orvig, C. Metal complexes of maltol and close analogues in medicinal inorganic chemistry. *Chemical Society Reviews*, 35(6):545-556, 2006.

40. Marwaha, S. S., Kaur, J., and Sodhi, G. S. Organomercury(II) complexes of kojic acid and maltol: Synthesis, characterization, and biological studies. *Journal of Inorganic Biochemistry*, 54(1):67-74, 1994.
41. Maurya, R. C., Bohre, P., Sahu, S., Martin, M. H., Sharma, A. K., and Vishwakarma, P. Oxoperoxomolybdenum(VI) complexes of catalytic and biomedical relevance: Synthesis, characterization, antibacterial activity and 3D-molecular modeling of some oxoperoxomolybdenum(VI) chelates in mixed (O, O) coordination environment involving maltol and β-diketoenolates. *Arabian Journal of Chemistry*, 9:S150-S160, 2016.
42. Orvig, C., Caravan, P., Gelmini, L., Glover, N., Herring, F. G., Li, H., McNeill, J. H., Rettig, S. J., and Setyawati, I. A. Reaction chemistry of BMOV, bis(maltolato)oxovanadium(IV), a potent insulin mimetic agent. *Journal of the American Chemical Society*, 117(51):12759-12770, 1995.
43. Thompson, K. H., Chiles, J., Yuen, V. G., Tse, J., McNeill, J. H., and Orvig, C. Comparison of anti-hyperglycemic effect amongst vanadium, molybdenum and other metal maltol complexes. *Journal of Inorganic Biochemistry*, 98(5):683-690, 2004.
44. Li, M., Ding, W., Baruah, B., Crans, D. C., and Wang, R. Inhibition of protein tyrosine phosphatase 1B and alkaline phosphatase by bis(maltolato)oxovanadium(IV). *Journal of Inorganic Biochemistry*, 102(10):1846-1853, 2008.
45. Barrio, D., Braziunas, M., Etcheverry, S., and Cortizo, A. Maltol complexes of vanadium(IV) and (V) regulate in vitro alkaline phosphatase activity and osteoblast-like cell growth. *Journal of Trace Elements in Medicine and Biology*, 11(2):110-115, 1997.
46. Passoni, L. C., Siddiqui, M. R. H., Steiner, A., and Kozhevnikov, I. V. Niobium peroxo compounds as catalysts for liquid-phase oxidation with hydrogen peroxide. *Journal of Molecular Catalysis A: Chemical*, 153(1-2):103-108, 2000.
47. Sheldrick, G. M. A short history of SHELX. *Acta Crystallographica Section A: Foundations of Crystallography*, 64(1):112-122, 2008.
48. Burnett, M. N. and Johnson, C. K. *ORTEP-III: Oak Ridge Thermal Ellipsoid Plot Program for Crystal Structure Illustrations*, Oak Ridge National Laboratory Report ORNL-6895, pages 1997-2002. Tennessee, 1996.

49. Frisch, M. J., Trucks, G.W., Schlegel, H. B., Scuseria, G. E., Robb, M., Cheeseman, J. R., Scalmani, G., Barone, V., Mennucci, B., Petersson, G. A., Nakatsuji, H. et al. *Gaussian 09* (Revision D.01); Gaussian. Inc. Wallingford CT, 2009.
50. Wang, Y., Verma, P., Jin, X., Truhlar, D. G., and He, X. Revised M06 density functional for main-group and transition-metal chemistry. *Proceedings of the National Academy of Sciences*, 115(41):10257-10262, 2018.
51. Zhao, Y. and Truhlar, D. G. The M06 suite of density functionals for main group thermochemistry, thermochemical kinetics, noncovalent interactions, excited states, and transition elements: two new functionals and systematic testing of four M06-class functionals and 12 other functionals. *Theoretical Chemistry Accounts*, 120:215-241, 2008.
52. Weigend, F. and Ahlrichs, R. Balanced basis sets of split valence, triple zeta valence and quadruple zeta valence quality for H to Rn: Design and assessment of accuracy. *Physical Chemistry Chemical Physics*, 7(18):3297-3305, 2005.
53. Fei, M. J., Chen, J. S., and Wang, X. Y. Biochemical properties and inhibition kinetics of phosphatase from wheat thylakoid membranes. *Journal of Integrative Plant Biology*, 48(3):294-299, 2006.
54. Bergmeyer, H. U., Bergmeyer, J., and Grassl, M. *Methods of Enzymatic Analysis.* Verlag Chemie, Weinheim, Deerfield Beach, 3rd edition, 1983.
55. Albrecht, R., Le Petit, J., Calvert, V., Terrom, G., and Périssol, C. Changes in the level of alkaline and acid phosphatase activities during green wastes and sewage sludge co-composting. *Bioresource Technology*, 101(1):228-233, 2010.
56. Ferreira, C. V., Taga, E. M., and Aoyama, H. Glycolytic intermediates as substrates of soybean acid phosphatase isoforms. *Plant Science*, 147(1):49-54, 1999.
57. Nelson, D. L., Cox, M. M., and Hoskins A. A. *Lehninger Principles of Biochemistry*, pages 802-812. Macmillan Learning, New York, 2021.
58. Bisswanger, H. *Enzyme Kinetics: Principles and Methods*. WILEY-VCH Verlag GmbH & Co. KGaA, Weinheim, Germany, 2008.
59. Atkins, P. and de Paula, J. *Atkins' Physical Chemistry*, pages 840-845. Oxford University Press, New York, 2006.
60. Greaves, S. J. and Griffith, W. P. Surface-enhanced raman spectroscopy (SERS) of ligands and their complexes on silver sols—I. Maltol, tropolone and their complexes with group VIII and group VI metals. *Polyhedron*, 7(19-20):1973-1979, 1988.

61. Case, D. R., Gonzalez, R., Zubieta, J., and Doyle, R. P. Synthesis, characterization, and cellular uptake of magnesium maltol and ethylmaltol complexes. *ACS Omega*, 6(44):29713-29723, 2021.
62. Sukhov, B. G., Mukha, S. A., Antipova, I. A., Medvedeva, S. A., Larina, L. I., Chipanina, N. N., Kazheva, O. N., Shilov, G. V., Dyachenko, O. A., and Trofimova, B. A. Stereoactive lone pair of electrons on bismuth(III): tris(3-hydroxy-2-methyl-4H-pyran-4-onato)bismuth(III). *Arkivoc*, 8(6):139-149, 2008.
63. Serafím, M. J., Bessler, K. E., Lemos, S. S., Sales, M. J., and Ellena, J. The preparation of new oxoniobium(V) complexes from hydrated niobium(V) oxide: The crystal and molecular structure of oxotris(2-pyridinolato-N-oxide)niobium(V). *Transition Metal Chemistry*, 32:112-116, 2007.
64. Bayot, D., Devillers, M., and Peeters, D. Vibrational spectra of eight-coordinate niobium and tantalum complexes with peroxo ligands: A theoretical simulation. *European Journal of Inorganic Chemistry*, 4118–4123, 2005.
65. Ni, Y., Wang, Y., and Kokot, S. Simultaneous kinetic-spectrophotometric determination of maltol and ethyl maltol in food samples by using chemometrics. *Food Chemistry*, 109(2):431-438, 2008.
66. Enyedy, É. A., Hollender, D., and Kiss, T. Lipophilicity of kinetically labile metal complexes through the example of antidiabetic Zn(II) and VO(IV) compounds. *Journal of Pharmaceutical and Biomedical Analysis*, 54(5):1073-1081, 2011.
67. Maniatakou, A., Makedonas, C., Mitsopoulou, C. A., Raptopoulou, C., Rizopoulou, I., Terzis, A., and Karaliota, A. Synthesis, structural and DFT studies of a peroxo-niobate complex of the biological ligand 2-quinaldic acid. *Polyhedron*, 27(16):3398-3408, 2008.
68. Gogoi, S. R., Boruah, J. J., Sengupta, G., Saikia, G., Ahmed, K., Bania, K. K., and Islam, N. S. Peroxoniobium(V)-catalyzed selective oxidation of sulfides with hydrogen peroxide in water: A sustainable approach. *Catalysis Science & Technology*, 5(1):595-610, 2015.
69. Fox, R. C. and Taylor, P. D. Efficient Syntheses of N-alkyl-3-hydroxy-2-methyl-4 (1H)-pyridinones from carbohydrate precursors. *Synthetic Communications*, 29(6):989-1001, 1999.
70. Buglyó, P., Kiss, T., Kiss, E., Sanna, D., Garribba, E., and Micera, G. Interaction between the low molecular mass components of blood serum and the VO(IV)–DHP

system (DHP= 1, 2-dimethyl-3-hydroxy-4 (1 H)-pyridinone). *Journal of the Chemical Society, Dalton Transactions*, (11):2275-2282, 2002.

71. Fregona, D., Faraglia, G., and Sitran, S. Tin and germanium complexes with maltol. *Journal of Coordination Chemistry*, 30(3-4):221-231, 1993.
72. Barret, M. C., Mahon, M. F., Molloy, K. C., Steed, J. W., and Wright, P. Synthesis and structural characterization of tin(II) and zinc(II) derivatives of cyclic α-hydroxyketones, including the structures of $Sn(maltol)_2$, $Sn(tropolone)_2$, $Zn(tropolone)_2$, and $Zn(hinokitiol)_2$. *Inorganic Chemistry*, 40(17):4384-4388, 2001.
73. Galešić, N., Brničević, N., Matković, B., Herceg, M., Zelenko, B., Šljukić, M., Prelesnik, B., and Herak, R. The crystal structure of ammonium oxobisoxalato-bisaquoniobate(V) trihydrate $NH_4[NbO(C_2O_4)_2(H_2O)_2]\cdot 3H_2O$ by neutron diffraction. *Journal of the Less Common Metals*, 51(2):259-270, 1977.
74. Bayot, D., Tinant, B., and Devillers, M. Homo-and heterobimetallic niobium^{v} and tantalum^{v} peroxo-tartrate complexes and their use as molecular precursors for Nb-Ta mixed oxides. *Inorganic Chemistry*, 44(5):1554-1562, 2005.
75. Bayot, D., Tinant, B., Mathieu, B., Declercq, J. P., and Devillers, M. Spectroscopic and structural characterizations of novel water-soluble peroxo[polyaminocarboxylato bis(N-oxido)]niobate(v) complexes. *European Journal of Inorganic Chemistry*, 2003(4):737-743, 2003.
76. Bayot, D., Degand, M., Tinant, B., and Devillers, M. Spectroscopic and structural characterizations of water-soluble peroxo complexes of niobium(V) with N-containing heterocyclic ligands. *Inorganica Chimica Acta*, 359(5):1390-1394, 2006.
77. Peters, K. G., Davis, M. G., Howard, B. W., Pokross, M., Rastogi, V., Diven, C., Greis, K. D., Eby-Wilkens, E., Maier, M., and Evdokimov, A. Mechanism of insulin sensitization by BMOV (bis maltolato oxo vanadium); unliganded vanadium (VO_4) as the active component. *Journal of Inorganic Biochemistry*, 96(2-3):321-330, 2003.
78. Lipscomb, W. N. and Sträter, N. Recent advances in zinc enzymology. *Chemical Reviews*, 96(7):2375-2434, 1996.
79. Wilcox, D. E. Binuclear metallohydrolases. *Chemical Reviews*, 96(7):2435-2458, 1996.
80. Cornish-Bowden, A. Current IUBMB recommendations on enzyme nomenclature and kinetics. *Perspectives in Science*, 1(1-6):74-87, 2014.

81. Duggleby, R. G. Determination of inhibition constants, I_{50} values and the type of inhibition for enzyme-catalyzed reactions. *Biochemical Medicine and Metabolic Biology*, 40(2), 204-212, 1988.
82. Cha, S. Tight-binding inhibitors–I: kinetic behavior. *Biochemical Pharmacology*, 24(23):2177-2185, 1975.
83. Vincent, J. B., Crowder, M. W., and Averill, B. A. Spectroscopic and kinetics studies of a high-salt-stabilized form of the purple acid phosphatase from bovine spleen. *Biochemistry*, 30(12):3025-3034, 1991.
84. Stankiewicz, P. J. and Gresser, M. J. Inhibition of phosphatase and sulfatase by transition-state analogs. *Biochemistry*, 27(1):206-212, 1988.
85. Heo, Y.-S., Ryu, J. M., Park, S. M., Park, J. H., Lee, H.-C., Hwang, K. Y., and Kim, J. S. Structural basis for inhibition of protein tyrosine phosphatases by Keggin compounds phosphomolybdate and phosphotungstate. *Experimental & Molecular Medicine*, 34(3):211-223, 2002.
86. Crans, D. C. In Tracey A. S. and Crans D. C., editors, *Vanadium Compounds: Chemistry, Biochemistry, and Therapeutic Applications*, pages 82-103. Oxford University Press, New York, 1998.
87. VanEtten, R. L., Waymack, P. P., and Rehkop, D. M. Transition metal ion inhibition of enzyme-catalyzed phosphate ester displacement reactions. *Journal of the American Chemical Society*, 96(21):6782-6785, 1974.
88. Soman, G., Chang, Y. C., and Graves, D. J. Effect of oxyanions of the early transition metals on rabbit skeletal muscle phosphorylase. *Biochemistry*, 22(21):4994-5000, 1983.
89. Hunt, D. F., Yates III, J. R., Shabanowitz, J., Zhu, N.-Z., Zirino, T., Averill, B. A., Daurat-Larroque, S. T., Shewale, J. G., Roberts, R. M., and Brew, K. Sequence homology in the metalloproteins; purple acid phosphatase from beef spleen and uteroferrin from porcine uterus. *Biochemical and Biophysical Research Communications*, 144(3):1154-1160, 1987.
90. Ketcham, C., Roberts, R., Simmen, R. C., and Nick, H. S. Molecular cloning of the type 5, iron-containing, tartrate-resistant acid phosphatase from human placenta. *Journal of Biological Chemistry*, 264(1):557-563, 1989.
91. Lord, D. K., Cross, N. C., Bevilacqua, M. A., Rider, S. H., Gorman, P. A., Groves, A. V., Moss, D. W., Sheer, D., and Cox, T. M. Type 5 acid phosphatase: Sequence,

expression and chromosomal localization of a differentiation-associated protein of the human macrophage. *European Journal of Biochemistry*, 189(2):287-293, 1990.

92. Gogoi, S. R., Ahmed, K., Saikia, G., and Islam, N. S. Macromolecular metal complexes of Nb^{V} as recoverable catalysts for selective and eco-compatible oxidation of organic sulfides in water. *Journal of the Indian Chemical Society*, 95:801-812, 2018.